The Interstellar Medium

16

Although most of the mass of the Milky Way Galaxy is condensed into stars, interstellar space is not completely empty. It contains *gas* and *dust* in the form both of individual clouds and of a diffuse medium. Interstellar space typically contains about one gas atom per cubic centimetre and 100 dust particles per cubic kilometre.

Altogether, about 10 % of the mass of the Milky Way consists of interstellar gas. Since the gas is strongly concentrated in the galactic plane and the spiral arms, in these regions there are many places where the quantities of stars and interstellar matter are about equal. The dust (a better name would be "smoke", since the particle sizes are much smaller than in terrestrial dust) constitutes about one percent of the gas. High-energy cosmic ray particles are mixed with the gas and dust. There is also a weak, but still very important, galactic magnetic field.

At present the most important observations of the interstellar medium are made at radio and infrared wavelengths, since the peak of the emission often lies at these wavelengths. But many forms of interstellar matter (such as solid bodies with diameters larger than 1 mm) would be almost impossible to detect on the basis of their emission or absorption. In principle, the mass of these forms of matter might be larger than the observed mass of all other forms put together. However, an upper limit on the total mass of interstellar matter, regardless of its form, can be derived on the basis of its gravitational effects. This is the *Oort limit*. The galactic gravitational field is determined by the distribution of matter. By observing the motions of stars perpendicular to the galactic plane, the vertical gravitational force and hence the amount of mass in the galactic plane can be determined. The result is that the local density within 1 kpc of the Sun is $(7.3–10.0) \times 10^{-21}$ kg m^{-3}. The density of known stars is $(5.9–6.7) \times 10^{-21}$ kg m^{-3} and that of known interstellar matter about 1.7×10^{-21} kg m^{-3}. Thus there is very little room for unknown forms of mass in the solar neighbourhood. However, the limit concerns only the dark matter concentrated in the galactic plane. There are indications that the Milky Way is surrounded by a spherical halo of dark matter (Chap. 18).

16.1 Interstellar Dust

The first clear evidence for the existence of interstellar dust was obtained around 1930. Before that, it had been generally thought that space is completely transparent and that light can propagate indefinitely without extinction.

In 1930 *Robert Trumpler* published his study of the space distribution of the open clusters. The absolute magnitudes M of the brightest stars could be estimated on the basis of the spectral type. Thus the distance r to the clusters could be calculated from the observed apparent magnitudes m of the bright stars:

$$m - M = 5 \lg \frac{r}{10\ \mathrm{pc}}. \qquad (16.1)$$

Trumpler also studied the diameters of the clusters. The linear diameter D is obtained from the

H. Karttunen et al. (eds.), *Fundamental Astronomy*, DOI 10.1007/978-3-662-53045-0_16

apparent angular diameter d by means of the formula

$$D = dr, \tag{16.2}$$

where r is the distance of the cluster.

It caught Trumpler's attention that the more distant clusters appeared to be systematically larger than the nearer ones (Fig. 16.1). Since this could hardly be true, the distances of the more distant clusters must have been overestimated. Trumpler concluded that space is not completely transparent, but that the light of a star is dimmed by some intervening material. To take this into account, (16.1) has to be replaced with (4.17)

$$m - M = 5 \lg \frac{r}{10\ \mathrm{pc}} + A, \tag{16.3}$$

where $A \geq 0$ is the extinction in magnitudes due to the intervening medium. If the opacity of the medium is assumed to be the same at all distances and in all directions, A can be written

$$A = ar, \tag{16.4}$$

where a is a constant. Trumpler obtained for the average value of a in the galactic plane, $a_{\mathrm{pg}} = 0.79$ mag/kpc, in photographic magnitudes. At present, a value of 2 mag/kpc is used for the average extinction. Thus the extinction over a 5 kpc path is already 10 magnitudes.

Extinction due to dust varies strongly with direction. For example, visible light from the galactic centre (distance 8–9 kpc) is dimmed by 30 magnitudes. Therefore the galactic centre cannot be observed at optical wavelengths.

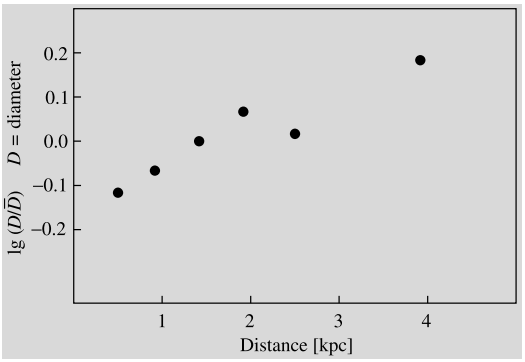

Fig. 16.1 The diameters of open star clusters calculated with the distance given by the formula (15.1) according to Trumpler (1930). The increase of the diameter with distance is not a real phenomenon, but an effect of interstellar extinction, which was discovered in this way

Extinction is due to dust grains that have diameters near the wavelength of the light. Such particles scatter light extremely efficiently. Gas can also cause extinction by scattering, but its scattering efficiency per unit mass is much smaller. The total amount of gas allowed by the Oort limit is so small that scattering by gas is negligible in interstellar space. (This is in contrast with the Earth's atmosphere, where air molecules make a significant contribution to the total extinction).

Interstellar particles can cause extinction in two ways:

1. In *absorption* the radiant energy is transformed into heat, which is then re-radiated at infrared wavelengths corresponding to the temperature of the dust particles.
2. In *scattering* the direction of light propagation is changed, leading to a reduced intensity in the original direction of propagation.

An expression for interstellar extinction will now be derived. The size, index of refraction and number density of the particles are assumed to be known. For simplicity we shall assume that all particles are spheres with the same radius a and the geometrical cross section πa^2. The true extinction cross section of the particles C_{ext} will be

$$C_{\mathrm{ext}} = Q_{\mathrm{ext}} \pi a^2, \tag{16.5}$$

where Q_{ext} is the extinction efficiency factor.

Let us consider a volume element with length $\mathrm{d}l$ and cross section $\mathrm{d}A$, normal to the direction of propagation (Fig. 16.2). It is assumed that the particles inside the element do not shadow each other. If the particle density is n, there are $n\,\mathrm{d}l\,\mathrm{d}A$ particles in the volume element and they will cover the fraction $\mathrm{d}\tau$ of the area $\mathrm{d}A$, where

$$\mathrm{d}\tau = \frac{n\,\mathrm{d}A\,\mathrm{d}l\,C_{\mathrm{ext}}}{\mathrm{d}A} = n\,C_{\mathrm{ext}}\,\mathrm{d}l.$$

In the length $\mathrm{d}l$ the intensity is thus changed by

$$\mathrm{d}I = -I\,\mathrm{d}\tau. \tag{16.6}$$

On the basis of (16.6) $\mathrm{d}\tau$ can be identified as the optical depth.

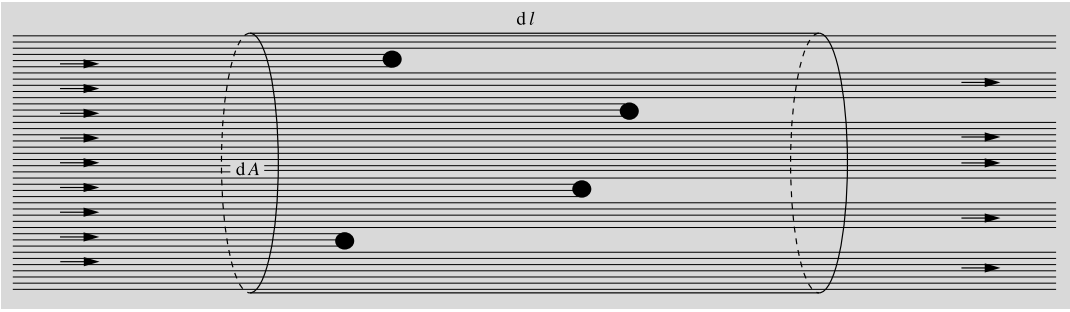

Fig. 16.2 Extinction by a distribution of particles. In the volume element with length dl and cross section dA, there are $n\,\mathrm{d}A\,\mathrm{d}l$ particles, where n is the particle density in the medium. If the extinction cross section of one particle is C_{ext}, the total area covered by the particles is $n\,\mathrm{d}A\,\mathrm{d}l\,C_{\mathrm{ext}}$. Thus the fractional decrease in intensity over the distance dl is $\mathrm{d}I/I = -n\,\mathrm{d}A\,\mathrm{d}l\,C_{\mathrm{ext}}/\mathrm{d}A = -n\,C_{\mathrm{ext}}\,\mathrm{d}l$

The total optical depth between the star and the Earth is

$$\tau(r) = \int_0^r \mathrm{d}\tau = \int_0^r n\,C_{\mathrm{ext}}\,\mathrm{d}l = C_{\mathrm{ext}}\overline{n}r,$$

where $\overline{n}$ is the average particle density along the given path. According to (4.18) the extinction in magnitudes is

$$A = (2.5\lg\mathrm{e})\tau,$$

and hence

$$A(r) = (2.5\lg\mathrm{e})C_{\mathrm{ext}}\overline{n}r. \qquad (16.7)$$

This formula can also be inverted to calculate $\overline{n}$, if the other quantities are known.

The extinction efficiency factor Q_{ext} can be calculated exactly for spherical particles with given radius a and refractive index m. In general,

$$Q_{\mathrm{ext}} = Q_{\mathrm{abs}} + Q_{\mathrm{sca}},$$

where

$$Q_{\mathrm{abs}} = \text{absorption efficiency factor},$$

$$Q_{\mathrm{sca}} = \text{scattering efficiency factor}.$$

If we define

$$x = 2\pi a/\lambda, \qquad (16.8)$$

where λ is the wavelength of the radiation, then

$$Q_{\mathrm{ext}} = Q_{\mathrm{ext}}(x, m). \qquad (16.9)$$

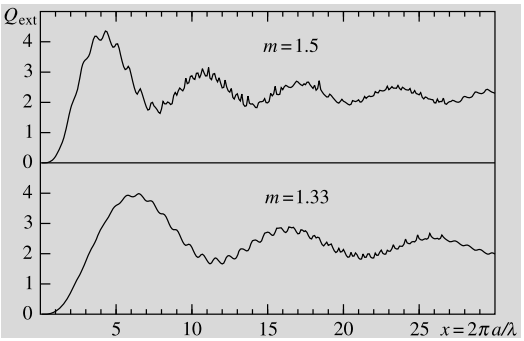

Fig. 16.3 Mie scattering: the extinction efficiency factor for spherical particles for the refractive indices $m = 1.5$ and $m = 1.33$ (refractive index of water). *The horizontal axis* is related to the size of the particle according to $x = 2\pi a/\lambda$, where a is the particle radius and λ, the wavelength of the radiation

The exact expression for Q_{ext} is a series expansion in x that converges more slowly for larger values of x. When $x \ll 1$, the process is called *Rayleigh scattering*; otherwise it is known as *Mie scattering*. Figure 16.3 shows Q_{ext} as a function of x for $m = 1.5$ and $m = 1.33$. For very large particles, ($x \gg 1$) $Q_{\mathrm{ext}} = 2$, as appears from Fig. 16.3. Purely geometrically one would have expected $Q_{\mathrm{ext}} = 1$; the two times larger scattering efficiency is due to the diffraction of light at the edges of the particle.

Other observable phenomena, apart from extinction, are also caused by interstellar dust. One of these is the *reddening* of the light of stars. (This should not be confused with the redshift of spectral lines.) Reddening is due to the fact

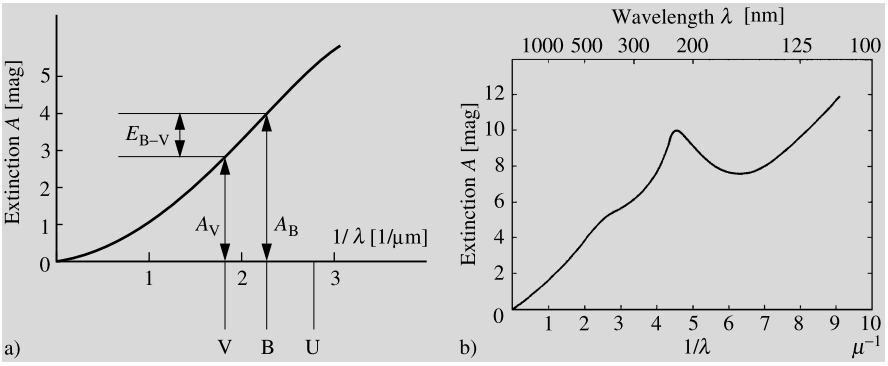

Fig. 16.4 (**a**) Schematic representation of the interstellar extinction. As the wavelength increases, the extinction approaches zero. (Drawing based on Greenberg, J.M. (1968): "Interstellar Grains", in *Nebulae and Interstellar Matter*, ed. by Middlehurst, B.M., Aller, L.H., Stars and Stellar Systems, Vol. VII (The University of Chicago Press, Chicago) p. 224). (**b**) Measured extinction curve, normalised to make $E_{B-V} = 1$. (Hoyle, F., Narlikar, J. (1980): *The Physics-Astronomy Frontier* (W.H. Freeman and Company, San Francisco) p. 156. Used by permission)

that the amount of extinction becomes larger for shorter wavelengths. Going from red to ultraviolet, the extinction is roughly inversely proportional to wavelength. For this reason the light of distant stars is redder than would be expected on the basis of their spectral class. The spectral class is defined on the basis of the relative strengths of the spectral lines which are not affected by extinction.

According to (4.20), the observed colour index $B - V$ of a star is

$$\begin{aligned} B - V &= M_B - M_V + A_B - A_B \\ &= (B - V)_0 + E_{B-V}, \end{aligned} \tag{16.10}$$

where $(B - V)_0$ is the *intrinsic colour* of the star and E_{B-V} the *colour excess*. As noted in Sect. 4.5 the ratio between the visual extinction A_V and the colour excess is approximately constant:

$$R = \frac{A_V}{E_{B-V}} = \frac{A_V}{A_B - A_V} \approx 3.0. \tag{16.11}$$

R does not depend on the properties of the star or the amount of extinction. This is particularly important in photometric distance determinations because of the fact that the colour excess E_{B-V} can be directly determined from the difference between the observed colour index $B - V$ and the intrinsic colour $(B - V)_0$ known from the spectral class. One can then calculate the extinction

$$A_V \approx 3.0\, E_{B-V} \tag{16.12}$$

and finally the distance. Since the interstellar medium is far from homogeneous, the colour excess method gives a much more reliable value than using some average value for the extinction in (4.18).

The wavelength dependence of the extinction, $A(\lambda)$, can be studied by comparing the magnitudes of stars of the same spectral class in different colours. These measurements have shown that $A(\lambda)$ approaches zero as λ becomes very large. In practice $A(\lambda)$ can be measured up to a wavelength of about two micrometres. The extrapolation to zero inverse wavelength is then fairly reliable. Figure 16.4(a) shows $A(\lambda)$ as a function of inverse wavelength. It also illustrates how the quantities A_V and E_{B-V}, which are needed in order to calculate the value of R, are obtained from this *extinction* or *reddening curve*. Figure 16.4(b) shows the observed extinction curve. The points in the ultraviolet ($\lambda \leq 0.3$ m) are based on rocket measurements.

It is clear from Fig. 16.4(b) that interstellar extinction is largest at short wavelengths in the ultraviolet and decreases for longer wavelengths. In the infrared it is only about ten percent of the optical extinction and in the radio region it is vanishingly small. Objects that are invisible in the opti-

cal region can therefore be studied at infrared and radio wavelengths.

Another observed phenomenon caused by dust is the *polarisation* of the light of the stars. Since spherical particles cannot produce any polarisation, the interstellar dust particles have to be non-spherical in shape. If the particles in a cloud are aligned by the interstellar magnetic field, they will polarise the radiation passing through the cloud. The degree of polarisation and its wavelength dependence give information on the properties of the dust particles. By studying the direction of polarisation in various directions, one can map the structure of the galactic magnetic field.

In the Milky Way interstellar dust is essentially confined to a very thin, about 100 pc, layer in the galactic plane. The dust in other spiral galaxies has a similar distribution and is directly visible as a dark band in the disk of the galaxy (Fig. 19.17 bottom). The Sun is located near the central plane of the galactic dust layer, and thus the extinction in the direction of the galactic plane is very large, whereas the total extinction towards the galactic poles may be less than 0.1 magnitudes. This is apparent in the distribution of galaxies in the sky: at high galactic latitudes, there are many galaxies, while near the galactic plane, there is a 20° zone where hardly any galaxies are seen. This empty region is called the *zone of avoidance*.

If a homogeneous dust layer gives rise to a total extinction of Δm magnitudes in the vertical direction, then according to Fig. 16.5, the total extinction at galactic latitude b will be

$$\Delta m(b) = \Delta m / \sin b. \tag{16.13}$$

If the galaxies are uniformly distributed in space, then in the absence of extinction, the number of galaxies per square degree brighter than the magnitude m would be

$$\lg N_0(m) = 0.6\, m + C, \tag{16.14}$$

where C is a constant (see Exercise 17.1). However, due to extinction, a galaxy that would otherwise have the apparent magnitude m_0 will have

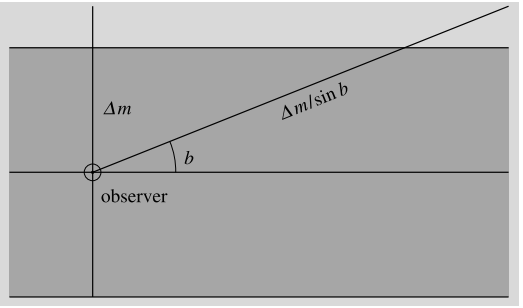

Fig. 16.5 In a homogeneous medium the extinction in magnitudes is proportional to the pathlength traversed. If the extinction in the direction of the galactic pole is Δm, then the extinction at the galactic latitude b will be $\Delta m / \sin b$

the magnitude

$$m(b) = m_0 + \Delta m(b) = m_0 + \Delta m / \sin b, \tag{16.15}$$

where b is the galactic latitude. Thus the observable number of galaxies at latitude b will be

$$\begin{aligned} \lg N(m, b) &= \lg N_0\big(m - \Delta m(b)\big) \\ &= 0.6\big(m - \Delta m(b)\big) + C \\ &= \lg N_0(m) - 0.6\Delta m(b) \end{aligned}$$

or

$$\lg N(m, b) = C' - 0.6\frac{\Delta m}{\sin b}, \tag{16.16}$$

where $C' = \lg N_0(m)$ does not depend on the galactic latitude. By making galaxy counts at various latitudes b, the extinction Δm can be determined. The value obtained from galaxy counts made at Lick Observatory is $\Delta m_{\mathrm{pg}} = 0.51$ mag.

The total vertical extinction of the Milky Way has also been determined from the colour excesses of stars. These investigations have yielded much smaller extinction values, about 0.1 mag. In the direction of the north pole, extinction is only 0.03 mag. The disagreement between the two extinction values is probably largely due to the fact that the dust layer is not really homogeneous. If the Sun is located in a local region of low dust content, the view towards the galactic poles might be almost unobstructed by dust.

Fig. 16.6 The Coalsack is a dark nebula next to the Southern Cross. (Photograph K. Mattila, Helsinki University)

Dark Nebulae Observations of other galaxies show that the dust is concentrated in the spiral arms, in particular at their inner edge. In addition dust is concentrated in individual clouds, which appear as star-poor regions or *dark nebulae* against the background of the Milky Way. Examples of dark nebulae are the Coalsack in the southern sky (Fig. 16.6) and the Horsehead nebula in Orion. Sometimes the dark nebulae form extended winding bands, and sometimes small, almost spherical, objects. Objects of the latter type are most easy to see against a bright background, e.g. a gas nebula (see Fig. 16.19). These objects have been named *globules* by *Bart J. Bok*, who put forward the hypothesis that they are clouds that are just beginning to contract into stars.

The extinction by a dark nebula can be illustrated and studied by means of a *Wolf diagram*, shown schematically in Fig. 16.7. The diagram is constructed on the basis of star counts. The number of stars per square degree in some magnitude interval (e.g. between magnitudes 14 and 15) in the cloud is counted and compared with the number outside the nebula. In the comparison area, the number of stars increases monotonically towards fainter magnitudes. In the dark nebula the numbers first increase in the same way, but beyond some limiting magnitude (10 in the figure)

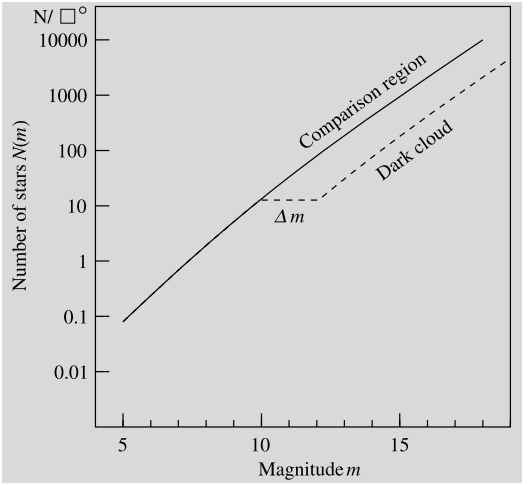

Fig. 16.7 Wolf diagram. *The horizontal coordinate* is the magnitude and *the vertical coordinate* is the number of stars per square degree in the sky brighter than that magnitude. A dark nebula diminishes the brightness of stars lying behind it by the amount Δm

the number of stars falls below that outside the cloud. The reason for this is that the fainter stars are predominantly behind the nebula, and their brightness is reduced by some constant amount Δm (2 magnitudes in the figure). The brighter stars are mostly in front of the nebula and suffer no extinction.

Reflection Nebulae If a dust cloud is near a bright star, it will scatter, i.e. reflect the light of the star. Thus individual dust clouds can sometimes be observed as bright *reflection nebulae*. Some 500 reflection nebulae are known.

The regions in the sky richest in reflection nebulae are the areas around the Pleiades and around the giant star Antares. Antares itself is surrounded by a large red reflection nebula. This region is shown in Fig. 16.8. Figure 16.9 shows the reflection nebula NGC 2068, which is located near a large, thick dust cloud a few degrees northwest of Orion's belt. It is one of the brightest reflection nebulae and the only one included in the Messier catalogue (M78). In the middle of the nebula there are two stars of about 11 magnitudes. The northern star illuminates the nebula, while the other one is probably in front of the nebula. Figure 16.10 shows the reflection nebula NGC 1435 around Merope in the Pleiades. Another bright and much-studied reflection nebula is NGC 7023 in Cepheus. It, too, is connected with a dark nebula. The illuminating star has emission lines in its spectrum (spectral type Be). Infrared stars have also been discovered in the area of the nebula, probably a region of star formation.

In 1922 *Edwin Hubble* published a fundamental investigation of bright nebulae in the Milky Way. On the basis of extensive photographic and spectroscopic observations, he was able to establish two interesting relationships. First he found that emission nebulae only occur near stars with spectral class earlier than B0, whereas reflection nebulae may be found near stars of spectral class B1 and later. Secondly Hubble discovered a relationship between the angular size R of the nebula and the apparent magnitude m of the illuminating star:

$$5 \lg R = -m + \text{const.} \qquad (16.17)$$

Thus the angular diameter of a reflection nebula is larger for a brighter illuminating star. Since the measured size of a nebula generally increases for longer exposures, i.e. fainter limiting surface brightness, the value of R should be defined to correspond to a fixed limiting surface brightness. The value of the constant in the Hubble relation depends on this limiting surface brightness. The Hubble relation for reflection nebulae is shown in Fig. 16.11, based on measurements by *Sidney van den Bergh* from Palomar Sky Atlas plates. Each point corresponds to a reflection nebula and the straight line represents the relation (16.17), where the value of the constant is 12.0 (R is given in arc minutes).

The Hubble relation can be derived theoretically, if it is assumed that the illumination of a dust cloud is inversely proportional to the square of the distance to the illuminating star, and that the dust clouds are uniformly distributed in space. The theoretical Hubble relation also gives an expression for the constant on the right-hand side, which involves the albedo and the phase function of the grains.

The observations of reflection nebulae show that the albedo of interstellar grains must be quite

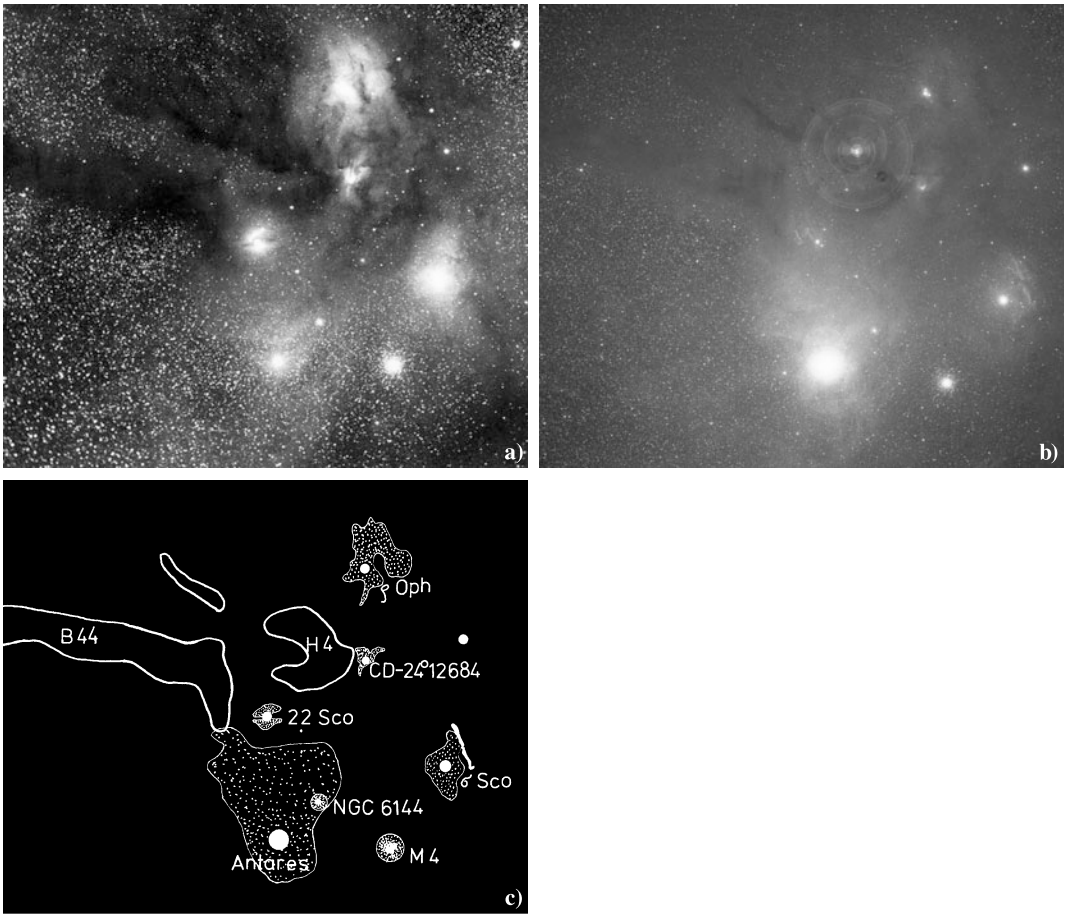

Fig. 16.8 Bright and dark nebulae in Scorpius and Ophiuchus. Photograph (**a**) was taken in the blue colour region, $\lambda = 350$–500 nm, and (**b**) in the red colour region, $\lambda = 600$–680 nm. (The sharp rings in **(b)** are reflections of Antares in the correction lens of the Schmidt camera.) The nebulae located in the area are identified in drawing (**c**). B44 and H4 are dark nebulae. There is a large reflection nebula around Antares, which is faintly visible in the blue **(a)**, but bright in the red **(b)** regions. Antares is very red (spectral class M1) and therefore the reflection nebula is also red. In contrast, the reflection nebulae around the blue stars ρ Ophiuchi (B2), CD-24° 12684 (B3), 22 Scorpii (B2) and σ Scorpii (B1) are blue and are visible only in **(a)**. In **(b)** there is an elongated nebula to the right of σ Scorpii, which is invisible in **(a)**. This is an emission nebula, which is very bright in the red hydrogen H_α line (656 nm). In this way reflection and emission nebulae can be distinguished by means of pictures taken in different wavelength regions. (Photograph **(a)** E. Barnard, and **(b)** K. Mattila)

high. It has not yet been possible to obtain its precise numerical value in this way, since the distances between the nebulae and their illuminating stars are not known well enough.

One may also consider the surface brightness of dark nebulae that are not close enough to a star to be visible as reflection nebulae. These nebulae will still reflect the diffuse galactic light from all the stars in the Milky Way. Calculations show that if the dust grains have a large albedo, then the reflected diffuse light should be bright enough to be observable, and it has indeed been observed. Thus the dark nebulae are not totally dark. The diffuse galactic light constitutes about 20–30 % of the total brightness of the Milky Way.

Dust Temperature In addition to scattering the interstellar grains also absorb radiation. The absorbed energy is re-radiated by the grains at infrared wavelengths corresponding to their

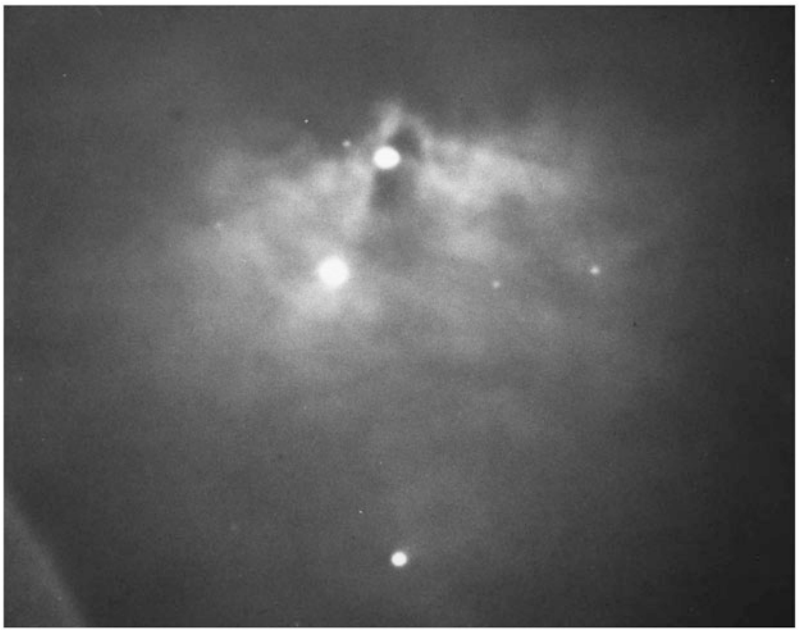

Fig. 16.9 The reflection nebula NGC 2068 (M78) in Orion. In the middle of the nebula there are two stars of about magnitude 11. The northern one (*at the top*) is the illuminating star, while the other one probably lies in the foreground. (Photography Lunar and Planetary Laboratory, Catalina Observatory)

Fig. 16.10 The reflection nebula NGC 1435 around Merope (23 Tau, spectral class B6) in the Pleiades. This figure should be compared with Fig. 16.1, where Merope is visible as the lowest of the bright stars in the Pleiades. (National Optical Astronomy Observatories, Kitt Peak National Observatory)

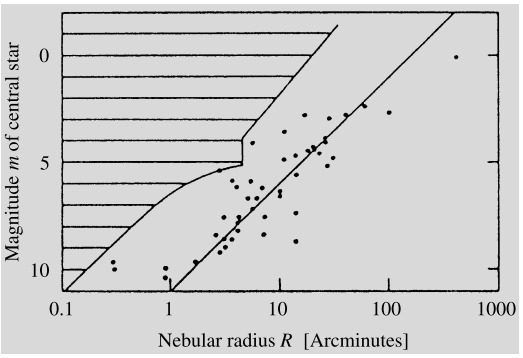

Fig. 16.11 The Hubble relation for reflection nebulae. *The horizontal axis* shows the radius R of the nebulae in arc minutes and *the vertical axis*, the (blue) apparent magnitude m of the central star. No measurements were made in the hatched region. (van den Bergh, S. (1966): Astron. J. **71**, 990)

temperatures. The temperature of dust in interstellar space (including dark nebulae) is about 10–20 K. The corresponding wavelength according to Wien's displacement law (5.21) is 300–150 μm. Near a hot star the temperature of the dust may be 100–600 K and the maximum emission is then at 30–5 μm. In H II regions the dust temperature is about 70–100 K.

The rapid development of infrared astronomy in the 1970's has brought all the above-mentioned dust sources within the reach of observations (Fig. 16.12). In addition infrared radiation from the nuclei of normal and active galaxies is largely thermal radiation from dust. Thermal dust emission is one of the most important sources of infrared radiation in astronomy.

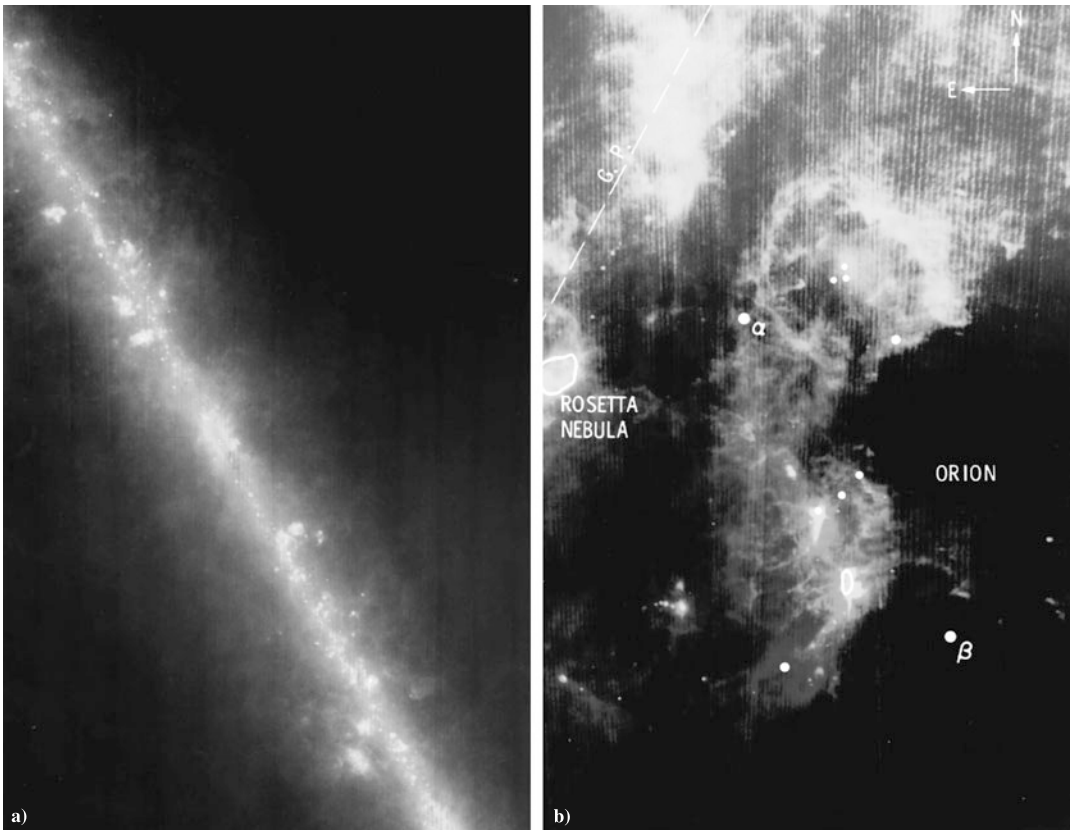

Fig. 16.12 Interstellar dust is best seen in infrared wavelengths. Two examples of the images by the IRAS satellite. (**a**) In a view towards the Galactic centre, the dust is seen to be concentrated in a narrow layer in the galactic plane. Several separate clouds are also seen. (**b**) Most of the constellation Orion is covered by a complex area of interstellar matter. The densest concentrations of dust below the centre of the image, are in the region of the Horsehead nebula and the Orion nebula. (Photos NASA)

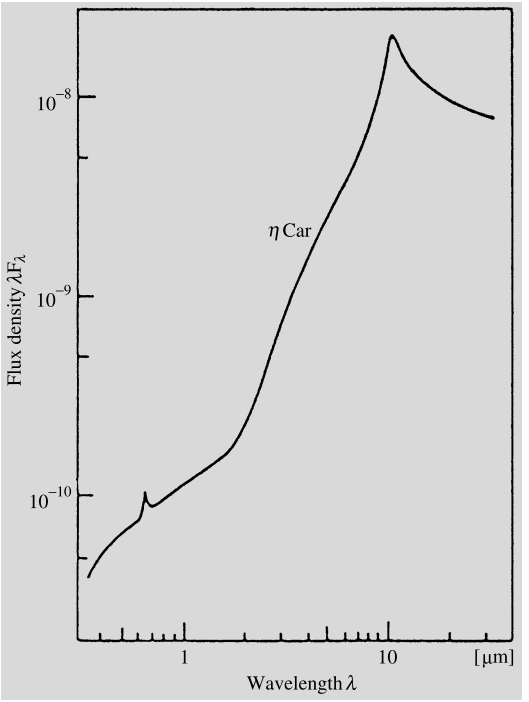

Fig. 16.13 More than 99 % of the radiation from the η Carinae nebula (Fig. 13.10) is in the infrared. The peak in the visual region is from the hydrogen H_α line (0.66 μm). In the infrared, the silicate emission from dust is evident at 10 μm. (Allen, D.A. (1975): *Infrared, the New Astronomy* (Keith Reid Ltd., Shaldon) p. 103)

One of the strongest infrared sources in the sky is the nebula around the star η Carinae. The nebula consists of ionised gas, but infrared radiation from dust is also clearly visible in its spectrum (Fig. 16.13). In even more extreme cases, the central star may be completely obscured, but revealed by the infrared emission from hot dust.

Composition and Origin of the Dust (Tables 16.1 and 16.2). From the peaks in the extinction curve, it may be concluded that interstellar dust contains water ice and silicates, and probably graphite as well. The sizes of the grains can be deduced from their scattering properties; usually they are smaller than one micrometre. The strongest scattering is due to grains of about 0.3 μm but smaller particles must also be present.

Dust grains are formed in the atmospheres of stars of late spectral types (K, M). Gas condenses into grains just as water in the Earth's atmosphere may condense into snow and ice. The grains are then expelled into interstellar space by the radiation pressure. Grains may also form in connection with star formation and possibly directly from atoms and molecules in interstellar clouds as well.

16.2 Interstellar Gas

The mass of gas in interstellar space is a hundred times larger than that of dust. Although there is more gas, it is less easily observed, since the gas does not cause a general extinction of light. In the optical region it can only be observed on the basis of a small number of spectral lines.

The existence of interstellar gas began to be suspected in the first decade of the 20th century, when in 1904 *Johannes Hartmann* observed that some absorption lines in the spectra of certain binary stars were not Doppler shifted by the motions of the stars like the other lines. It was concluded that these absorption lines were formed in gas clouds in the space between the Earth and the stars. In some stars there were several lines, apparently formed in clouds moving with different velocities. The strongest lines in the visible region are those of neutral sodium and singly ionised calcium (Fig. 16.14). In the ultraviolet region, the lines are more numerous. The strongest one is the hydrogen Lyman α line (121.6 nm).

On the basis of the optical and ultraviolet lines, it has been found that many atoms are ionised in interstellar space. This ionisation is mainly due to ultraviolet radiation from stars and, to some extent, to ionisation by cosmic rays. Since the density of interstellar matter is very low, the free electrons only rarely encounter ions, and the gas remains ionised.

About thirty elements have been discovered by absorption line observations in the visible and ultraviolet region. With a few exceptions, all elements from hydrogen to zinc (atomic number 30) and a few additional heavier elements have been detected (Table 16.3). Like in the stars, most of

Table 16.1 Main properties of interstellar gas and dust

Property	Gas	Dust
Mass fraction	10 %	0.1 %
Composition	H I, H II, H_2 (70 %) He (28 %) C, N, O, Ne, Na, Mg, Al, Si, S, … (2 %)	Solid particles $d \approx 0.1$–1 μm H_2O (ice), silicates, graphite + impurities
Particle density	1 /cm^3	10^{-13} /cm^3 = 100 /km^3
Mass density	10^{-21} kg/m^3	10^{-23} kg/m^3
Temperature	100 K (H I), 10^4 K (H II) 50 K (H_2)	10–20 K
Method of study	Absorption lines in stellar spectra. Optical: Ca I, Ca II, Na I, K I, Ti II, Fe I, CN, CH, CH^+ Ultraviolet: H_2, CO, HD Radio lines: hydrogen 21 cm emission and absorption; H II, He II, C II recombination lines; molecular emission and absorption lines OH, H_2CO, NH_3, H_2O, CO, H_2C_2HCN, C_2H_5OH	Absorption and scattering of starlight. Interstellar reddening Interstellar polarisation Thermal infrared emission

the mass is hydrogen (about 70 %) and helium (almost 30 %). On the other hand, heavy elements are significantly less abundant than in the Sun and other population I stars. It is thought that they have been incorporated into dust grains, where they do not produce any absorption lines. The element abundances in the interstellar medium (gas + dust) would then be normal, although the interstellar gas is depleted in heavy elements. This interpretation is supported by the observation that in regions where the amount of dust is smaller than usual, the element abundances in the gas are closer to normal.

Atomic Hydrogen Ultraviolet observations have provided an excellent way of studying interstellar *neutral hydrogen*. The strongest interstellar absorption line, as has already been mentioned, is the hydrogen Lyman α line (Fig. 16.15). This line corresponds to the transition of the electron in the hydrogen atom from a state with principal quantum number $n = 1$ to one with $n = 2$. The conditions in interstellar space are such that almost all hydrogen atoms are in the ground state with $n = 1$. Therefore the Lyman α line is a strong absorption line, whereas the Balmer absorption lines, which arise from the excited initial state $n = 2$, are unobservable. (The Balmer lines are strong in stellar atmospheres with temperatures of about 10,000 K, where a large number of atoms are in the first excited state.)

The first observations of the interstellar Lyman α line were made from a rocket already in 1967. More extensive observations comprising 95 stars were obtained by the OAO 2 satellite. The distances of the observed stars are between 100 and 1000 parsecs.

Comparison of the Lyman α observations with observations of the 21 cm neutral hydrogen line have been especially useful. The distribution of neutral hydrogen over the whole sky has been mapped by means of the 21 cm line. However, the distances to nearby hydrogen clouds are difficult to determine from these observations. In the

Table 16.2 Phenomena caused by the interstellar medium

Observable phenomenon	Cause
Interstellar extinction and polarisation	Non-spherical dust grains aligned by magnetic field
Dark nebulae, uneven distribution of stars and galaxies	Dust clouds
Interstellar absorption lines in stellar spectra	Atoms and molecules in the interstellar gas
Reflection nebulae	Interstellar dust clouds illuminated by nearby stars
Emission nebulae or H II regions (optical, infrared and radio emission)	Interstellar gas and dust cloud, where a nearby hot star ionises the gas and heats the dust to 50–100 K
Optical galactic background (diffuse galactic light)	Interstellar dust illuminated by the integrated light of all stars
Galactic background radiation:	
(a) short wavelength ($\lesssim 1$ m)	Free–free emission from hot interstellar gas
(b) long wavelength ($\gtrsim 1$ m)	Synchrotron radiation from cosmic ray electrons in the magnetic field
Galactic 21 cm emission	Cold (100 K) interstellar neutral hydrogen clouds (H I regions)
Molecular line emission (extended)	Giant molecular clouds (masses even 10^5–$10^6\ M_\odot$), dark nebulae
Point-like OH, H_2O and SiO sources	Maser sources near protostars and long-period variables

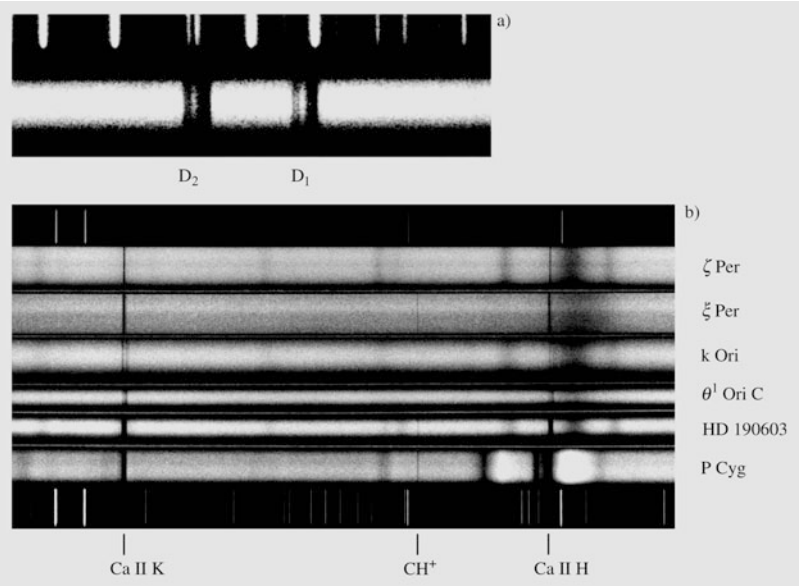

Fig. 16.14 (**a**) The D lines D_1 and D_2 of interstellar sodium (rest wavelengths 589.89 and 589.00 nm) in the spectrum of the star HD 14134. Both lines consist of two components formed in the gas clouds of two spiral arms. The radial velocity difference of the arms is about 30 km/s. (Mt. Wilson Observatory). (**b**) The interstellar absorption lines of ionised calcium Ca II and ionised methylidyne CH^+ in the spectra of several stars. The emission spectrum of iron is shown for comparison in **(a)** and **(b)**. (Lick Observatory)

Lyman α observations one usually knows the distance to the star in front of which the absorbing clouds must lie.

The average gas density within about 1 kpc of the Sun derived from the Lyman α observations is 0.7 atoms/cm^3. Because the interstellar Lyman α line is so strong, it can be observed even in the spectra of very nearby stars. For example, it has been detected by the Copernicus satellite in the spectrum of Arcturus, whose distance is only 11 parsecs. The deduced density of neutral hydrogen between the Sun and Arcturus is 0.02–0.1 atoms/cm^3. Thus the Sun is situated in a clearing in the interstellar medium, where the

Table 16.3 Element abundances in the interstellar medium towards ζ Ophiuchi and in the Sun. The abundances are given relative to that of hydrogen, which has been defined to be 1,000,000. An asterisk (*) means that the abundance has been determined from meteorites. The last column gives the ratio of the abundances in the interstellar medium and in the Sun

Atomic number	Name	Chemical symbol	Interstellar abundance	Solar abundance	Abundance ratio
1	Hydrogen	H	1,000,000	1,000,000	1.00
2	Helium	He	85,000	85,000	$\approx$1
3	Lithium	Li	0.000051	0.00158*	0.034
4	Beryllium	Be	$<$0.000070	0.000012	$<$5.8
5	Boron	B	0.000074	0.0046*	0.016
6	Carbon	C	74	370	0.20
7	Nitrogen	N	21	110	0.19
8	Oxygen	O	172	660	0.26
9	Fluorine	F	–	0.040	–
10	Neon	Ne	–	83	–
11	Sodium	Na	0.22	1.7	0.13
12	Magnesium	Mg	1.05	35	0.030
13	Aluminium	Al	0.0013	2.5	0.00052
14	Silicon	Si	0.81	35	0.023
15	Phosphorus	P	0.021	0.27	0.079
16	Sulfur	S	8.2	16	0.51
17	Chlorine	Cl	0.099	0.45	0.22
18	Argon	Ar	0.86	4.5	0.19
19	Potassium	K	0.010	0.11	0.094
20	Calcium	Ca	0.00046	2.1	0.00022
21	Scandium	Sc	–	0.0017	–
22	Titanium	Ti	0.00018	0.055	0.0032
23	Vanadium	V	$<$0.0032	0.013	$<$0.25
24	Chromium	Cr	$<$0.002	0.50	$<$0.004
25	Manganese	Mn	0.014	0.26	0.055
26	Iron	Fe	0.28	25	0.011
27	Cobalt	Co	$<$0.19	0.032	$<$5.8
28	Nickel	Ni	0.0065	1.3	0.0050
29	Copper	Cu	0.00064	0.028	0.023
30	Zinc	Zn	0.014	0.026	0.53

density is less than one tenth of the average density.

If a hydrogen atom in its ground state absorbs radiation with a wavelength smaller than 91.2 nm, it will be ionised. Knowing the density of neutral hydrogen, one can calculate the expected distance a 91.2 nm photon can propagate before being absorbed in the ionisation of a hydrogen atom. Even in the close neighbourhood of the Sun, where the density is exceptionally low, the mean free path of a 91.2 nm photon is only about a parsec and that of a 10 nm photon a few hundred parsecs. Thus only the closest neighbourhood of the Sun can be studied in the extreme ultraviolet (XUV) spectral region.

The Hydrogen 21 cm Line The spins of the electron and proton in the neutral hydrogen

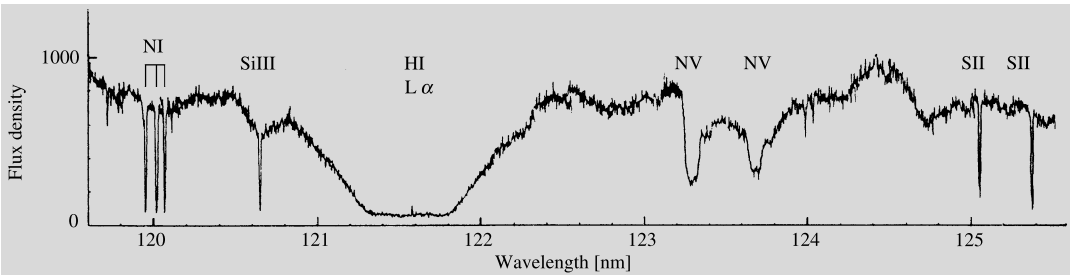

Fig. 16.15 Interstellar absorption lines in the ultraviolet spectrum of ζ Ophiuchi. The strongest line is the hydrogen Lyman α line (equivalent width, more than 1 nm). The observations were made with the Copernicus satellite. (Morton, D.C. (1975): Astrophys. J. **197**, 85)

atom in the ground state may be either parallel or opposite. The energy difference between these two states corresponds to the frequency of 1420.4 MHz. Thus transitions between these two hyperfine structure energy levels will give rise to a spectral line at the wavelength of 21.049 cm (Fig. 5.8). The existence of the line was theoretically predicted by *Hendrick van de Hulst* in 1944, and was first observed by *Harold Ewen* and *Edward Purcell* in 1951. Studies of this line have revealed more about the properties of the interstellar medium than any other method—one might even speak of a special branch of 21 cm astronomy. The spiral structure and rotation of the Milky Way and other galaxies can also be studied by means of the 21 cm line.

Usually the hydrogen 21 cm line occurs in emission. Because of the large abundance of hydrogen, it can be observed in all directions in the sky. Some observed 21 cm line profiles are shown in Fig. 16.16. Rather than frequency or wavelength, the radial velocity calculated from the Doppler formula is plotted on the horizontal axis. This is because the broadening of the 21 cm spectral line is always due to gas motions either within the cloud (turbulence) or of the cloud as a whole. The vertical axis is mostly plotted in terms of the antenna temperature T_A (see Chap. 5), the usual radio astronomical measure of intensity. The brightness temperature of an extended source is then $T_\mathrm{b} = T_\mathrm{A}/\eta_\mathrm{B}$, where η_B is the beam efficiency of the antenna.

For the 21 cm line $h\nu/k = 0.07$ K, and thus $h\nu/kT \ll 1$ for all relevant temperatures. One

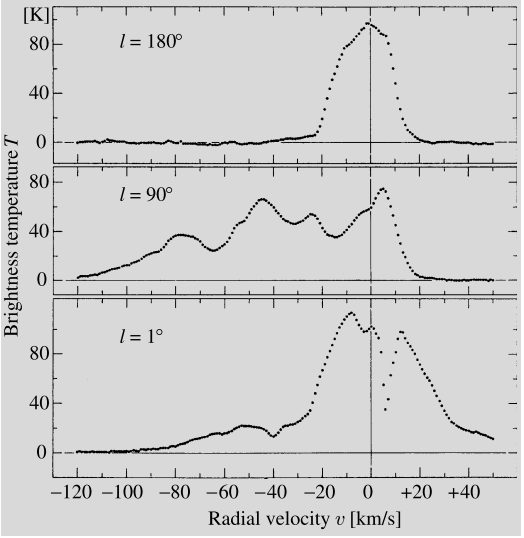

Fig. 16.16 Hydrogen 21 cm emission line profiles in the galactic plane at longitude 180°, 90° and 1° (in the direction $l = 0°$ there is strong absorption). *The horizontal axis* gives the radial velocity according to the Doppler formula, *the vertical axis* gives the brightness temperature. (Burton, W.B. (1974): "The Large Scale Distribution of Neutral Hydrogen in the Galaxy", in *Galactic and Extra-Galactic Radio Astronomy*, ed. by Verschuur, G.L., Kellermann, K.I. (Springer, Berlin, Heidelberg, New York) p. 91)

may therefore use the Rayleigh–Jeans approximation (5.24)

$$I_\nu = \frac{2\nu^2 kT}{c^2}. \tag{16.18}$$

In the solution of the equation of radiative transfer (5.42) the intensity can thus be directly related to a corresponding temperature. By definition, I_ν is related to the brightness temperature T_b, and

the source function S_ν is related to the excitation temperature $T_{\rm exc}$, i.e.

$$T_{\rm b} = T_{\rm exc}\left(1 - {\rm e}^{-\tau_\nu}\right). \tag{16.19}$$

In certain directions in the Milky Way there is so much hydrogen along the line of sight that the 21 cm line is optically thick, $\tau_\nu \gg 1$. In that case

$$T_{\rm b} = T_{\rm exc}, \tag{16.20}$$

i.e. the brightness temperature immediately yields the excitation temperature of the cloud. This is often referred to as the *spin temperature* $T_{\rm S}$.

The excitation temperature need not always agree with the kinetic temperature of the gas. However, in the present case the population numbers of the hyperfine levels are determined by mutual collisions of hydrogen atoms: the time between collisions is 400 years on the average, whereas the time for spontaneous radiative transitions is 11 million years; thus the excitation temperature will be the same as the kinetic temperature. The observed temperature is $T \approx 125$ K.

The distance to a source cannot be obtained directly from the observed emission. Thus one can only study the number of hydrogen atoms in a cylinder with a 1 cm^2 base area extending from the observer to outside the Milky Way along the line of sight. This is called the *projected* or *column density* and is denoted by N. One may also consider the column density $N(v)\,{\rm d}v$ of atoms with velocities in the interval $[v, v + {\rm d}v]$.

It can be shown that if the gas is optically thin, the brightness temperature in a spectral line is directly proportional to the column density N of atoms with the corresponding radial velocity. Hence, if the diameter L of a cloud along the line of sight is known, the gas density can be determined from the observed line profile:

$$n = N/L.$$

The diameter L can be obtained from the apparent diameter, if the distance and shape of the cloud are assumed known.

The distances of clouds can be determined from their radial velocities by making use of the rotation of the Milky Way (Sect. 18.3). Thus if the observed peaks in the 21 cm line profiles (Fig. 16.16) are due to individual clouds, their distances and densities can be obtained. Since radio observations are not affected by extinction, it has been possible in this way to map the density distribution of neutral hydrogen in the whole galactic plane. The resulting distribution, based on observations at Leiden and Parkes, is shown in Fig. 16.17. It appears that the Milky Way is a spiral galaxy and that the interstellar hydrogen is concentrated in the spiral arms. The average density of interstellar hydrogen is 1 atom/cm^3, but the distribution is very inhomogeneous. Typically the hydrogen forms denser regions, a few parsecs in size, where the densities may be 10–100 atoms/cm^3. Regions where the hydrogen is predominantly neutral are known as *H I regions* (in contrast to H II regions of ionised hydrogen).

The hydrogen 21 cm line may also occur in absorption, when the light from a bright radio source, e.g. a quasar, passes through an intervening cloud. The same cloud may give rise to both an absorption and an emission spectrum. In that case the temperature, optical thickness and hydrogen content of the cloud can all be derived.

Like interstellar dust hydrogen is concentrated in a thin disk in the galactic plane. The thickness of the hydrogen layer is about twice that of the dust or about 200 pc.

H II Regions In many parts of space hydrogen does not occur as neutral atoms, but is ionised. This is true in particular around hot O stars, which radiate strongly in the ultraviolet. If there is enough hydrogen around such a star, it will be visible as an emission nebula of ionised hydrogen. Such nebulae are known as *H II region* (Figs. 16.18 and 16.19).

A typical emission nebula is the great nebula in Orion, M42. It is visible even to the unaided eye, and is a beautiful sight when seen through a telescope. In the middle of the nebula there is a group of four hot stars known as the Trapezium, which can be distinguished inside the bright nebula, even with a small telescope. The Trapezium stars emit strong ultraviolet radiation, which keeps the gas nebula ionised.

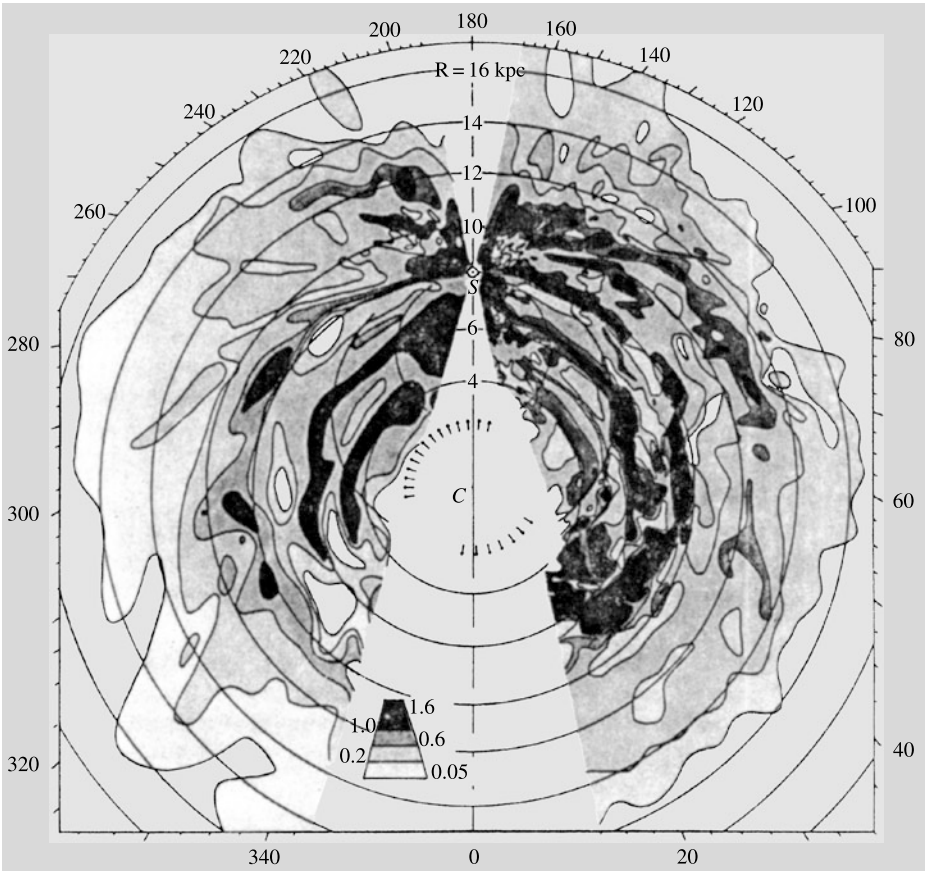

Fig. 16.17 The distribution of neutral hydrogen in the galaxy from the Leiden and Parkes surveys. The density is given in atoms/cm^3. (Oort, J.H., Kerr, P.T., Westerhout, G.L. (1958): Mon. Not. R. Astron. Soc. **118**, 379)

Unlike a star a cloud of ionised gas has a spectrum dominated by a few narrow emission lines. The continuous spectrum of H II regions is weak. In the visible region the hydrogen Balmer emission lines are particularly strong. These are formed when a hydrogen atom recombines into an excited state and subsequently returns to the ground state via a sequence of radiative transitions. Typically a hydrogen atom in a H II region remains ionised for several hundred years. Upon recombination it stays neutral for some months, before being ionised again by a photon from a nearby star.

The number of recombinations per unit time and volume is proportional to the product of the densities of electrons and ions,

$$n_{\mathrm{rec}} \propto n_{\mathrm{e}} n_{\mathrm{i}}. \tag{16.21}$$

In completely ionised hydrogen, $n_{\mathrm{e}} = n_{\mathrm{i}}$, and hence

$$n_{\mathrm{rec}} \propto n_{\mathrm{e}}^2. \tag{16.22}$$

Most recombinations will include the transition $n = 3 \rightarrow 2$, i.e. will lead to the emission of a H_α photon. Thus the surface brightness of a nebula in the H_α line will be proportional to the *emission measure*,

$$EM = \int n_{\mathrm{e}}^2 \, \mathrm{d}l, \tag{16.23}$$

where the integral is along the line of sight through the nebula.

The ionisation of a helium atom requires more energy than that of a hydrogen atom, and thus regions of ionised helium are formed only around

Fig. 16.18 The great nebula in Orion (M42, NGC 1976). The nebula gets its energy from newly formed hot stars. The dark regions are opaque dust clouds in front of the nebula. Radio and infrared observations have revealed a rich molecular cloud behind the nebula (Fig. 16.20). *In the upper part* of this picture is the gas nebula NGC 1977, *in the lower part* the bright star ι Orionis. (Lick Observatory)

the hottest stars. In these cases, a large H II region will surround a smaller central He^{+} or He^{++} region. The helium lines will then be strong in the spectrum of the nebula.

Although hydrogen and helium are the main constituents of clouds, their emission lines are not always strongest in the spectrum. At the beginning of this century it was even suggested that some strong unidentified lines in the spectra of nebulae were due to the new element nebulium. However, in 1927 *Ira S. Bowen* showed that they were *forbidden lines* of ionised oxygen and nitrogen, O^{+}, O^{++} and N^{+}. Forbidden lines are extremely difficult to observe in the laboratory, because their transition probabilities are so small that at laboratory densities the ions are de-excited by collisions before they have had time to radiate. In the extremely diffuse interstellar gas, collisions are much less frequent, and thus there is a chance that an excited ion will make the transition to a lower state by emitting a photon.

Because of interstellar extinction, only the nearest H II regions can be studied in visible light. At infrared and radio wavelengths much more distant regions can be studied. The most important lines at radio wavelengths are recombination lines of hydrogen and helium; thus the hydrogen transition between energy levels 110 and 109 at 5.01 GHz has been much studied. These lines are also important because with their help radial velocities, and hence (using the galactic rotation

Fig. 16.19 The Lagoon nebula (M8, NGC 6523) in Sagittarius. This H II region contains many stars of early spectral types and stars that are still contracting towards the main sequence. Small, round dark nebulae, globules, are also visible against the bright background. These are presumably gas clouds in the process of condensation into stars. (National Optical Astronomy Observatories, Kitt Peak National Observatory)

law), distances of H II regions can be determined, just as for neutral hydrogen.

The physical properties of H II regions can also be studied by means of their continuum radio emission. The radiation is due to bremsstrahlung or free–free emission from the electrons. The intensity of the radiation is proportional to the emission measure *EM* defined in (16.23). H II regions also have a strong infrared continuum emission. This is thermal radiation from dust inside the nebula.

H II regions are formed when a hot O or B star begins to ionise its surrounding gas. The ionisation steadily propagates away from the star. Because neutral hydrogen absorbs ultraviolet radiation so efficiently, the boundary between the H II region and the neutral gas is very sharp. In a homogeneous medium the H II region around a single star will be spherical, forming a *Strömgren sphere*. For a B0 V star the radius of the Strömgren sphere is 50 pc and for an A0 V star only 1 pc.

The temperature of a H II region is higher than that of the surrounding gas, and it therefore tends to expand. After millions of years, it will have become extremely diffuse and will eventually merge with the general interstellar medium.

16.3 Interstellar Molecules

The first *interstellar molecules* were discovered in 1937–1938, when molecular absorption lines were found in the spectra of some stars. Three simple diatomic molecules were detected: *methylidyne* CH, its positive ion CH^+ and *cyanogen* CN. A few other molecules were later discovered by the same method in the ultraviolet. Thus *molecular hydrogen* H_2 was discovered in the early 1970's, and *carbon monoxide*, which had been discovered by radio observations, was also detected in the ultraviolet. Molecular hydrogen is the most abundant interstellar molecule, followed by carbon monoxide.

Molecular Hydrogen The detection and study of molecular hydrogen has been one of the most important achievements of UV astronomy. Molecular hydrogen has a strong absorption band at 105 nm, which was first observed in a rocket experiment in 1970 by *George R. Carruthers*, but more extensive observations could only be made with the Copernicus satellite. The observations showed that a significant fraction of interstellar hydrogen is molecular, and that this fraction increases strongly for denser clouds with higher ex-

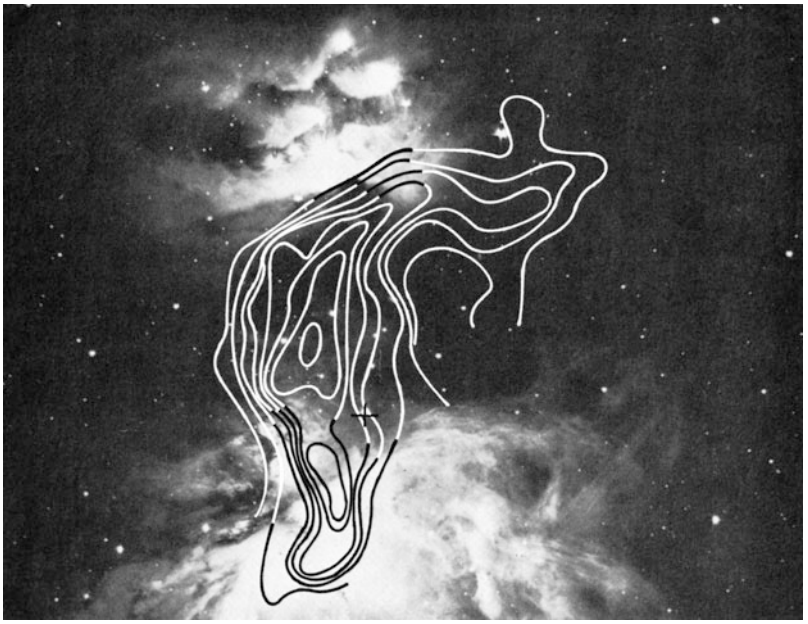

Fig. 16.20 Radio map of the distribution of carbon monoxide $^{13}C^{16}O$ in the molecular cloud near the Orion nebula. *The curves* are lines of constant intensity. (Kutner, M.L., Evans II, N.J., Tucker, K.D. (1976): Astrophys. J. **209**, 452)

tinction. In clouds with visual extinction larger than one magnitude essentially all the hydrogen is molecular.

Hydrogen molecules are formed on the surface of interstellar grains, which thus act as a chemical catalyst. Dust is also needed to shield the molecules from the stellar UV radiation, which would otherwise destroy them. Molecular hydrogen is thus found where dust is abundant. It is of interest to know whether gas and dust are well mixed or whether they form separate clouds and condensations.

UV observations have provided a reliable way of comparing the distribution of interstellar gas and dust. The amount of dust between the observer and a star is obtained from the extinction of the stellar light. Furthermore, the absorption lines of atomic and molecular hydrogen in the ultraviolet spectrum of the same star can be observed. Thus the total amount of hydrogen (atomic + molecular) between the observer and the star can also be determined.

Observations indicate that the gas and dust are well mixed. The amount of dust giving rise to one magnitude visual extinction corresponds to 1.9×10^{21} hydrogen atoms (one molecule is counted as two atoms). The mass ratio of gas and dust obtained in this way is 100.

Radio Spectroscopy Absorption lines can only be observed if there is a bright star behind the molecular cloud. Because of the large dust extinction, no observations of molecules in the densest clouds can be made in the optical and ultraviolet spectral regions. Thus only radio observations are possible for these objects, where molecules are especially abundant.

Radio spectroscopy signifies an immense step forward in the study of interstellar molecules. In the early 1960's, it was still not believed that there might be more complicated molecules than diatomic ones in interstellar space. It was thought that the gas was too diffuse for molecules to form and that any that formed would be destroyed by ultraviolet radiation. The first molecular radio line, the hydroxyl radical OH, was discovered in 1963. Many other molecules have been discovered since then. By 2002, about 130 molecules had been detected, the heaviest one being the 13-atom molecule $HC_{11}N$.

Molecular lines in the radio region may be observed either in absorption or in emission. Radiation from diatomic molecules like CO (see Fig. 16.20) may correspond to three kinds of transitions. (1) *Electron transitions* correspond to changes in the electron cloud of the molecule. These are like the transitions in single atoms, and

Table 16.4 Some molecules observed in the interstellar medium

Molecule	Name	Year of discovery
Discovered in the optical and ultraviolet region:		
CH	methylidyne	1937
CH^+	methylidyne ion	1937
CN	cyanogen	1938
H_2	hydrogen molecule	1970
CO	carbon monoxide	1971
Discovered in the radio region:		
OH	hydroxyl radical	1963
CO	carbon monoxide	1970
CS	carbon monosulfide	1971
SiO	silicon monoxide	1971
SO	sulfur monoxide	1973
H_2O	water	1969
HCN	hydrogen cyanide	1970
NH_3	ammonia	1968
H_2CO	formaldehyde	1969
HCOOH	formic acid	1975
HCCNC	isocyanoacetylene	1991
C_2H_4O	vinyl alcohol	2001
H_2CCCC	cumulene carbene	1991
$(CH_3)_2O$	dimethyl ether	1974
C_2H_5OH	ethanol	1975
$HC_{11}N$	cyanopentacetylene	1981

their wavelengths lie in the optical or ultraviolet region. (2) *Vibrational transitions* correspond to changes in the vibrational energy of the molecule. Their energies are usually in the infrared region. (3) Most important for radio spectroscopy are the *rotational transitions*, which are changes in the rotational energy of the molecule. Molecules in their ground state do not rotate, i.e. their angular momentum is zero, but they may be excited and start rotating in collisions with other molecules. For example, carbon sulfide CS returns to its ground state in a few hours by emitting a millimetre region photon.

A number of interstellar molecules are listed in Table 16.4. Many of them have only been detected in the densest clouds (mainly the Sagittarius B2 cloud at the galactic centre), but others are very common. The most abundant molecule H_2 cannot be observed at radio wavelengths, because it has no suitable spectral lines. The next most abundant molecules are carbon monoxide CO, the hydroxyl radical OH and ammonia NH_3, although their abundance is only a small fraction of that of hydrogen. However, the masses of interstellar clouds are so large that the number of molecules is still considerable. (The Sagittarius B2 cloud contains enough ethanol, C_2H_5OH, for 10^{28} bottles of vodka.)

Both the formation and survival of interstellar molecules requires a higher density than is common in interstellar clouds; thus they are most common in dense clouds. Molecules are formed in collisions of atoms or simpler molecules or catalysed on dust grains. Molecular clouds must also contain a lot of dust to absorb the ultraviolet radiation entering from outside that otherwise would disrupt the molecules. The most suitable conditions are thus found inside dust and molecular clouds near dense dark nebulae and H II regions.

Most of the molecules in Table 16.4 have only been detected in dense molecular clouds occurring in connection with H II regions. Almost every molecule yet discovered has been detected in Sagittarius B2 near the galactic centre. Another very rich molecular cloud has been observed near the H II region Orion A. In visible light this region has long been known as the Orion nebula M42 (Fig. 16.18). Inside the actual H II regions there are no molecules, since they would be rapidly dissociated by the high temperature and strong ultraviolet radiation. Three types of molecular sources have been found near H II regions (Fig. 16.21):

1. Large gas and dust envelopes around the H II region.
2. Small dense clouds inside these envelopes.
3. Very compact OH and H_2O maser sources.

The large envelopes have been discovered primarily by CO observations. OH and H_2CO have also been detected. Like in the dark nebulae the gas in these clouds is probably mainly molecular hydrogen. Because of the large size and density ($n \approx 10^3$–10^4 molecules/cm^3) of these clouds, their masses are very large, 10^5 or even 10^6 solar

Table 16.5 The five phases of interstellar gas

		T [K]	n [cm^{-3}]
1.	Very cold molecular gas clouds (mostly hydrogen H_2)	20	$\gtrsim 10^3$
2.	Cold gas clouds (mostly atomic neutral hydrogen)	100	20
3.	Warm neutral gas enveloping the cooler clouds	6000	0.05–0.3
4.	Hot ionised gas (mainly H II regions around hot stars)	8000	>0.5
5.	Very hot and diffuse ionised coronal gas, ionised and heated by supernova explosions	10^6	10^{-3}

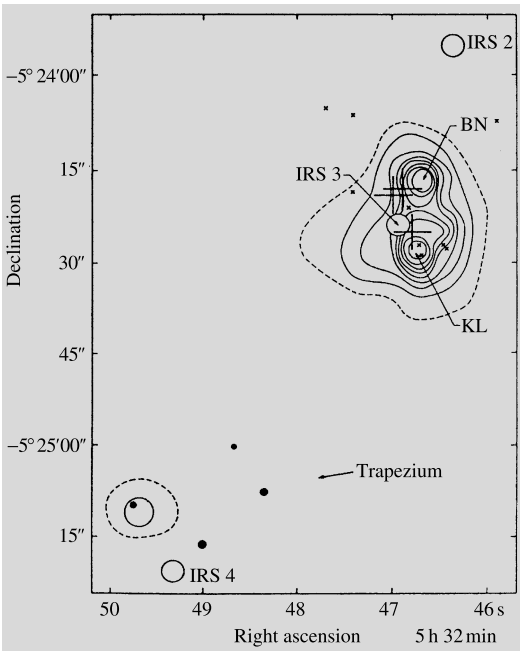

Fig. 16.21 Infrared map of the central part of the Orion nebula. *In the lower part* are the four Trapezium stars. *Above* is an infrared source of about 0.5″ diameter, the Kleinmann–Low nebula (KL). BN is an infrared point source, the Becklin–Neugebauer object. Other infrared sources are denoted IRS. *The large crosses* indicate OH masers and *the small crosses* H_2O masers. On the scale of Fig. 16.18 this region would only be a few millimetres in size. (Goudis, C. (1982): The Orion Complex: A Case Study of Interstellar Matter (Reidel, Dordrecht) p. 176)

masses (Sgr B2). They are among the most massive objects in the Milky Way. The dust in molecular clouds can be observed on the basis of its thermal radiation. Its peak falls at wavelengths of 10–100 μm, corresponding to a dust temperature of 30–300 K.

Some interstellar clouds contain very small *maser sources*. In these the emission lines of OH, H_2O and SiO may be many million times stronger than elsewhere. The diameter of the radiating regions is only about 5–10 au. The conditions in these clouds are such that radiation in some spectral lines is amplified by stimulated emission as it propagates through the cloud. Hydroxyl and water masers occur in connection with dense H II regions and infrared sources, and appear to be related to the formation of protostars. In addition maser emission (OH, H_2O and SiO) occurs in connection with Mira variables and some red supergiant stars. This maser emission comes from a molecule and dust envelope around the star, which also gives rise to an observable infrared excess.

16.4 The Formation of Protostars

The mass of the Milky Way is about 10^{11} solar masses. Since its age is about 10^{10} years, stars have been forming at the average rate of $10\,M_\odot$ per year. This estimate is only an upper limit for the present rate, because earlier the rate of star formation must have been much higher. Since the lifetime of O stars is only about a million years, a better estimate of the star formation rate can be made, based on the observed number of O stars. Accordingly, it has been concluded that at present, new stars are forming in the Milky Way at a rate of about three solar masses per year.

Stars are now believed to form inside large dense interstellar clouds mostly located in the spiral arms of the Galaxy. Under its own gravity, a cloud begins to contract and fragment into parts that will become protostars. The observations seem to indicate that stars are not formed individually, but in larger groups. Young stars are

found in open clusters and in loose associations, typically containing a few hundred stars which must have formed simultaneously.

Theoretical calculations confirm that the formation of single stars is almost impossible. An interstellar cloud can contract only if its mass is large enough for gravity to overwhelm the pressure. As early as in the 1920's, James Jeans calculated that a cloud with a certain temperature and density can condense only if its mass is high enough. If the mass is too small the pressure of the gas is sufficient to prevent the gravitational contraction. The limiting mass is the Jeans mass (Sect. 6.11), given by

$$M_{\mathrm{J}} \approx 3 \times 10^4 \sqrt{\frac{T^3}{n}}\, M_{\odot},$$

where n is the density in atoms/m^3 and T the temperature.

In a typical interstellar neutral hydrogen cloud $n = 10^6$ and $T = 100$ K, giving the Jeans mass, $30{,}000\, M_{\odot}$. In the densest dark clouds $n = 10^{12}$ and $T = 10$ K and hence, $M_{\mathrm{J}} = 1\, M_{\odot}$.

It is thought that star formation begins in clouds of a few thousand solar masses and diameters of about 10 pc. The cloud begins to contract, but does not heat up because the liberated energy is carried away by radiation. As the density increases, the Jeans mass thus decreases. Because of this, separate condensation nuclei are formed in the cloud, which go on contracting independently: the cloud *fragments*. Fragmentation is further advanced by the increasing rotation velocity. The original cloud has a certain angular momentum which is conserved during the contraction; thus the angular velocity must increase.

This contraction and fragmentation continues until the density becomes so high that the individual fragments become optically thick. The energy liberated by the contraction can then no longer escape, and the temperature will begin to rise. In consequence the Jeans mass begins to increase, further fragmentation ceases and the rising pressure in existing fragments stops their contraction. Some of the protostars formed in this way may still be rotating too rapidly. These may split into two, thus forming double systems. The further evolution of protostars has been described in Sect. 11.2.

Although the view that stars are formed by the collapse of interstellar clouds is generally accepted, many details of the fragmentation process are still highly conjectural. Thus the effects of rotation, magnetic fields and energy input are very imperfectly known. Why a cloud begins to contract is also not certain; one theory is that passage through a spiral arm compresses clouds and triggers contraction (see Sect. 17.4). This would explain why young stars are predominantly found in the spiral arms of the Milky Way and other galaxies. The contraction of an interstellar cloud might also be initiated by a nearby expanding H II region or supernova explosion.

Star formation can be observed particularly well in the infrared, since the temperatures of the condensing clouds and protostars are of the order 100–1000 K and the infrared radiation can escape even the densest dust clouds. For example, in connection with the Orion nebula there is a large cloud of hydrogen, found in radio observations, containing small infrared sources. E.g. the Becklin–Neugebauer object has a temperature of a couple of hundred kelvins but a luminosity that is thousandfold compared with the Sun. It is a strong H_2O maser source, located next to a large H II region.

16.5 Planetary Nebulae

Bright regions of ionised gas do not occur only in connection with newly formed stars, but also around stars in late stages of their evolution. The *planetary nebulae* are gas shells around small hot blue stars. As we have seen in connection with stellar evolution, instabilities may develop at the stage of helium burning. Some stars begin to pulsate, while in others the whole outer atmosphere may be violently ejected into space. In the latter case, a gas shell expanding at 20–30 km/s will be formed around a small and hot (50,000–100,000 K) star, the core of the original star.

The expanding gas in a planetary nebula is ionised by ultraviolet radiation from the central

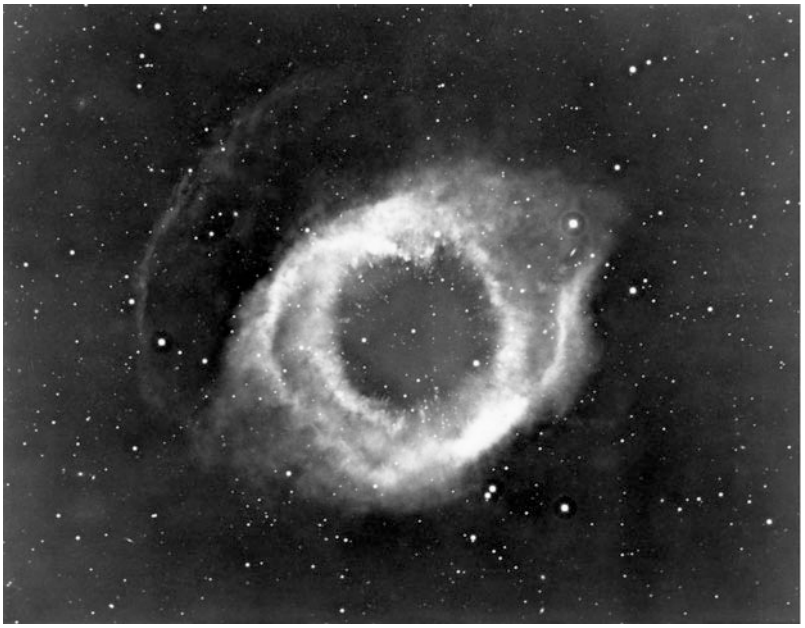

Fig. 16.22 The Helix nebula (NGC 7293). The planetary nebulae are formed during the final stages of evolution of solar-type stars. The centrally visible star has ejected its outer layers into space. (National Optical Astronomy Observatories, Kitt Peak National Observatory)

star, and its spectrum contains many of the same bright emission lines as that of an H II region. Planetary nebulae are, however, generally much more symmetrical in shape than most H II regions, and they expand more rapidly. For example, the well-known Ring nebula in Lyra (M57) has expanded visibly in photographs taken at 50-year intervals. In a few ten thousand years, the planetary nebulae disappear in the general interstellar medium and their central stars cool to become white dwarfs.

The planetary nebulae were given their name in the 19th century, because certain small nebulae visually look quite like planets such as Uranus. The apparent diameter of the smallest known planetary nebulae is only a few arc seconds, whereas the largest ones (like the Helix nebula) may be one degree in diameter (Fig. 16.22).

The brightest emission lines are often due to forbidden transitions, like in H II regions. For example, the green colour of the central parts of the Ring nebula in Lyra is due to the forbidden lines of doubly ionised oxygen at 495.9 and 500.7 nm. The red colour of the outer parts is due to the hydrogen Balmer α line (656.3 nm) and the forbidden lines of ionised nitrogen (654.8 nm, 658.3 nm).

The total number of planetary nebulae in the Milky Way has been estimated to be 50,000. About 2000 have actually been observed.

16.6 Supernova Remnants

In Chap. 11 we have seen that massive stars end their evolution in a supernova explosion. The collapse of the stellar core leads to the violent ejection of the outer layers, which then remain as an expanding gas cloud.

About 120 *supernova remnants* (SNR's) have been discovered in the Milky Way. Some of them are optically visible as a ring or an irregular nebula (e.g. the Crab nebula; see Fig. 16.23), but most are detectable only in the radio region (because radio emission suffers no extinction).

In the radio region the SNR's are extended sources similar to H II regions. However, unlike H II regions the radiation from SNR's is often polarised. Another characteristic difference between these two kinds of sources is that whereas the radio brightness of H II regions grows or remains constant as the frequency increases, that of SNR's falls off almost linearly (in a $\log I_\nu - \log \nu$ diagram) with increasing frequency (Fig. 16.24).

These differences are due to the different emission processes in H II regions and in SNR's.

Fig. 16.23 The Crab nebula (M1, NGC 1952) in Taurus is the remnant of a supernova explosion observed in 1054. The photograph was taken at red wavelengths. The nebula is also a strong radio source. Its energy source is the central rapidly rotating neutron star, pulsar, which is the collapsed core of the original star. (Palomar Observatory)

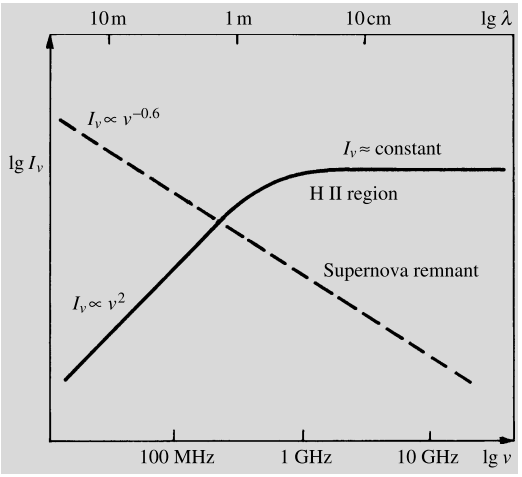

Fig. 16.24 The radio spectra of typical H II regions and supernova remnants. The radiation of H II regions is thermal and obeys the Rayleigh–Jeans law, $I \propto \nu^2$, at wavelengths larger than 1 m. In supernova remnants the intensity decreases with increasing frequency. (After Scheffler, H., Elsässer, H. (1987): *Physics of the Galaxy and the Interstellar Matter* (Springer, Berlin, Heidelberg, New York))

In an H II region, the radio emission is free–free radiation from the hot plasma. In a SNR it is *synchrotron radiation* from relativistic electrons moving in spiral orbits around the magnetic field lines. The synchrotron process gives rise to a continuous spectrum extending over all wavelength regions. For example, the Crab nebula looks blue or green in colour photographs because of optical synchrotron radiation.

In the Crab nebula red filaments are also visible against the bright background. Their emission is principally in the hydrogen H_α line. The hydrogen in a SNR is not ionised by a central star as in the H II regions, but by the ultraviolet synchrotron radiation.

The supernova remnants in the Milky Way fall into two classes. One type has a clearly ring-like structure (e.g. Cassiopeia A or the Veil nebula in Cygnus; see Fig. 16.25); another is irregular and bright at the middle (like the Crab nebula). In the remnants of the Crab nebula type there is always a rapidly rotating pulsar at the centre. This pulsar provides most of the energy of the remnant by continuously injecting relativistic electrons into the cloud. The evolution of this type of SNR reflects that of the pulsar and for this reason has a time scale of a few ten thousand years.

Ring-like SNR's do not contain an energetic pulsar; their energy comes from the actual supernova explosion. After the explosion, the cloud expands at a speed of 10,000–20,000 km/s. About

Fig. 16.25 The Veil nebula (NGC 6960 *at the right*, NGC 6992 *at the left*) in Cygnus is the remnant of a supernova explosion which occurred several ten thousand years ago. (Mt. Wilson Observatory)

50–100 years after the explosion the remnant begins to form a spherical shell as the ejected gas starts to sweep up interstellar gas and to slow down in its outer parts. The swept-up shell expands with a decreasing velocity and cools until, after about 100,000 years, it merges into the interstellar medium. The two types of supernova remnants may be related to the two types (I and II) of supernovae.

Box 16.1 (Synchrotron Radiation) Synchrotron radiation was first observed in 1948 by *Frank Elder*, *Robert Langmuir* and *Herbert Pollack*, who were experimenting with an electron synchrotron, in which electrons were accelerated to relativistic energies in a magnetic field. It was observed that the electrons radiated visible light in a narrow cone along their momentary direction of motion. In astrophysics synchrotron radiation was first invoked as an explanation of the radio emission of the Milky Way, discovered by *Karl Jansky* in 1931. This radiation had a spectrum and a large metre-wave brightness temperature (more than 10^5 K) which were inconsistent with ordinary thermal free-free emission from ionised gas. In 1950 *Hannes Alfvén* and *Nicolai Herlofson* as well as *Karl-Otto Kiepenheuer* proposed that the galactic radio background was due to synchrotron radiation. According to Kiepenheuer the high-energy cosmic ray electrons would emit radio radiation in the weak galactic mag-

netic field. This explanation has turned out to be correct. Synchrotron radiation is also an important emission process in supernova remnants, radio galaxies and quasars. It is *a non-thermal* radiation process, i.e. the energy of the radiating electrons is not due to thermal motions.

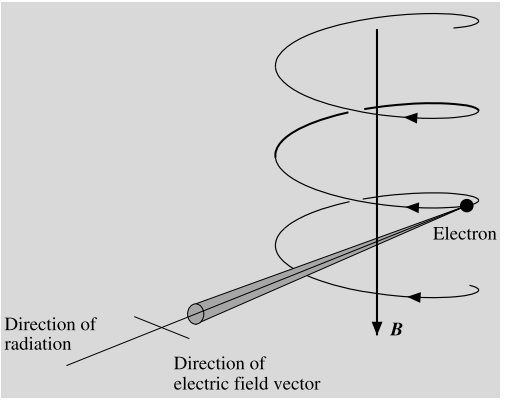

The emission of synchrotron radiation. A charged particle (electron) propagating in a magnetic field moves in a spiral. Because of the centripetal acceleration, the particle emits electromagnetic radiation

The origin of synchrotron radiation is schematically shown in the figure. The magnetic field forces the electron to move in a spiral orbit. The electron is thus constantly accelerated and will emit electromagnetic radiation. According to the special theory of relativity, the emission from a relativistic electron will be concentrated in a narrow cone. Like the beam from a lighthouse, this cone sweeps across the observer's field of vision once for each revolution. Thus the observer sees a sequence of radiation flashes of very short duration compared with their interval. (In the total emission of a large number of electrons, separate flashes cannot be distinguished.) When this series of pulses is represented as a sum of different frequency components (Fourier transform), a broad spectrum is obtained with a maximum at

$$\nu_{\max} = a B_{\perp} E^2,$$

where $B_{\perp}$ is the magnetic field component perpendicular to the velocity of the electron, and E its energy, a is a constant of proportionality.

The table gives the frequency and wavelength of the maximum as functions of the electron energy for the typical galactic field strength 0.5 nT:

$\lambda_{\max}$	$\nu_{\max}$ [Hz]	E [eV]
300 nm	10^{15}	6.6×10^{12}
30 μm	10^{13}	6.6×10^{11}
3 mm	10^{11}	6.6×10^{10}
30 cm	10^{9}	6.6×10^{9}
30 m	10^{7}	6.6×10^{8}

To produce even radio synchrotron radiation, very energetic electrons are required, but these are known to be present in the cosmic radiation. In the optical galactic background radiation, the contribution from synchrotron radiation is negligible, but, for example, in the Crab nebula, a significant part of the optical emission is due to this mechanism.

16.7 The Hot Corona of the Milky Way

As early as 1956 *Lyman Spitzer* showed that the Milky Way has to be surrounded by a large envelope of very hot gas (Fig. 16.26). Almost two decades later the Copernicus satellite, whose scientific program was directed by Spitzer, found evidence for this kind of gas, which began to be called *galactic coronal gas*, in analogy with the solar corona. The satellite observed emission lines of e.g. five times ionised oxygen (O VI), four times ionised nitrogen (N V) and triply ionised carbon (C IV). The formation of these lines requires a high temperature (100,000–1,000,000 K), and a high temperature is also indicated by the broadening of the lines.

Galactic coronal gas is distributed through the whole Milky Way and extends several thousand parsecs from the galactic plane. Its density is only of the order of 10^{-3} atoms/cm^3 (recall that the mean density in the galactic plane is 1 atom/cm^3). Thus coronal gas forms a kind of background sea, from which the denser and cooler forms of interstellar matter, such as neutral hydrogen and molecular clouds, rise as islands. In the early 1980's the IUE satellite also

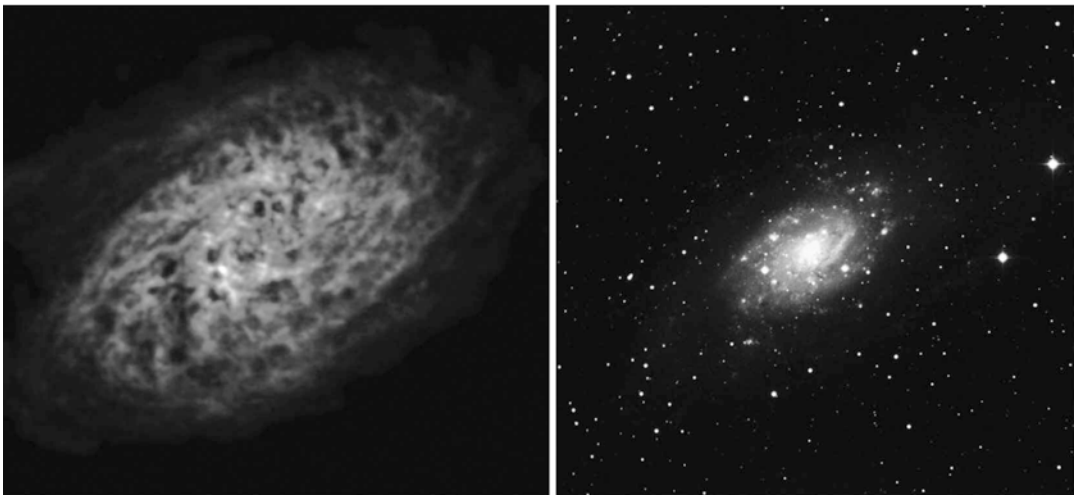

Fig. 16.26 Galaxy's hot corona. NGC 2403 is a spiral galaxy, similar to our Milky Way. *On the right*, it is photographed in visual light. *On the left*, in a VLA radio image, on the same scale with the optical image, a large hydrogen corona is seen around the galaxy. Large holes created by supernova explosions are seen in the gas corona. (Image NRAO/AUI and Tom Oosterloo, Astron, The Netherlands)

detected similar coronae in the Large Magellanic Cloud and in the spiral galaxy M100. Coronal gas is probably quite a common and important form of matter in galaxies.

Supernova explosions are probably the source of both coronal gas and its energy. When a supernova explodes, it forms a hot bubble in the surrounding medium. The bubbles from neighbouring supernovae will expand and merge, forming a foamlike structure. In addition to supernovae, stellar winds from hot stars may provide some of the energy of the coronal gas.

16.8 Cosmic Rays and the Interstellar Magnetic Field

Cosmic Rays Elementary particles and atomic nuclei reaching the Earth from space are called *cosmic rays*. They occur throughout interstellar space with an energy density of the same order of magnitude as that of the radiation from stars. Cosmic rays are therefore important for the ionisation and heating of interstellar gas.

Since cosmic rays are charged, their direction of propagation in space is constantly changed by the magnetic field. Their direction of arrival therefore gives no information about their place of origin. The most important properties of cosmic rays that can be observed from the Earth are their particle composition and energy distribution. As noted in Sect. 3.6, these observations have to be made in the upper atmosphere or from satellites, since cosmic ray particles are destroyed in the atmosphere.

The main constituent of the cosmic rays (about 90 %) is hydrogen nuclei or protons. The second most important constituent (about 9 %) is helium nuclei or α particles. The rest of the particles are electrons and nuclei more massive than helium.

Most cosmic rays have an energy smaller than 10^9 eV. The number of more energetic particles drops rapidly with increasing energy. The most energetic protons have an energy of 10^{20} eV, but such particles are very rare—the energy of one such proton could lift this book about one centimetre. (The largest particle accelerators reach "only" energies of 10^{12} eV.)

The distribution of low-energy (less than 10^8 eV) cosmic rays cannot be reliably determined from the Earth, since solar "cosmic rays", high-energy protons and electrons formed in solar flares fill the solar system and strongly affect the motion of low-energy cosmic rays.

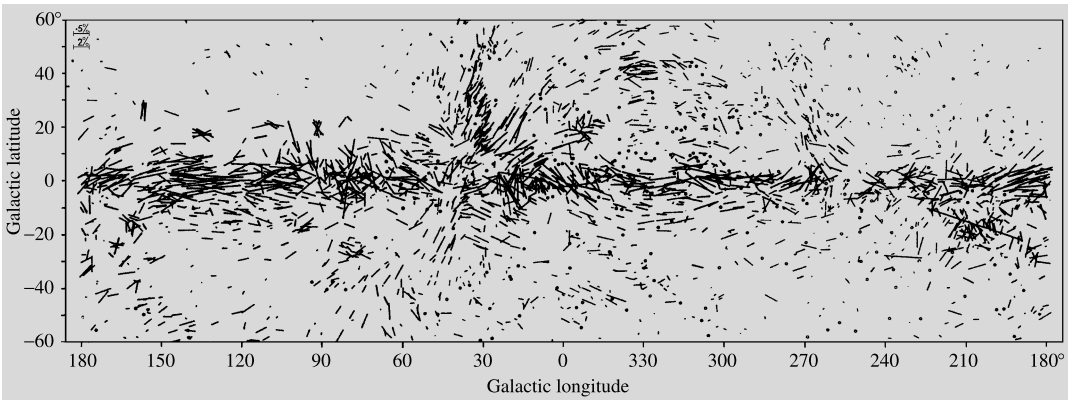

Fig. 16.27 The polarisation of starlight. *The dashes* give the direction and degree of the polarisation. *The thinner dashes* correspond to stars with polarisation smaller than 0.6 %; *the thicker dashes* to stars with larger polarisation. The scale is shown in *the upper left-hand corner*. Stars with polarisation smaller than 0.08 % are indicated by *a small circle*. (Mathewson, D.S., Ford, V.L. (1970): Mem. R.A.S. **74**, 139)

The distribution of cosmic rays in the Milky Way can be directly inferred from gamma-ray and radio observations. The collisions of cosmic ray protons with interstellar hydrogen atoms gives rise to pions which then decay to form a gamma-ray background. The radio background is formed by cosmic ray electrons which emit synchrotron radiation in the interstellar magnetic field.

Both radio and gamma-ray emission are strongly concentrated in the galactic plane. From this it has been concluded that the sources of cosmic rays must also be located in the galactic plane. In addition there are individual peaks in the backgrounds around known supernova remnants. In the gamma-ray region such peaks are observed at e.g. the Crab nebula and the Vela pulsar; in the radio region the North Polar Spur is a large, nearby ring-like region of enhanced emission.

Apparently a large fraction of cosmic rays have their origin in supernovae. An actual supernova explosion will give rise to energetic particles. If a pulsar is formed, observations show that it will accelerate particles in its surroundings. Finally the shock waves formed in the expanding supernova remnant will also give rise to relativistic particles.

On the basis of the relative abundances of various cosmic ray nuclei, it can be calculated how far they have travelled before reaching the Earth. It has been found that typical cosmic ray protons have travelled for a period of a few million years (and hence also a distance of a few million light-years) from their point of origin. Since the diameter of the Milky Way is about 100,000 light-years, the protons have crossed the Milky Way tens of times in the galactic field.

The Interstellar Magnetic Field The strength and direction of the *interstellar magnetic field* are difficult to determine reliably. Direct measurements are impossible, since the magnetic fields of the Earth and the Sun are much stronger. However, using various sources it has been possible to deduce the existence and strength of the field.

We have already seen that interstellar grains give rise to interstellar polarisation. In order to polarise light, the dust grains have to be similarly oriented; this can only be achieved by a general magnetic field. Figure 16.27 shows the distribution of interstellar polarisation over the sky. Stars near each other generally have the same polarisation. At low galactic latitudes the polarisation is almost parallel to the galactic plane, except where one is looking along a spiral arm.

More precise estimates of the strength of the magnetic field can be obtained from the rotation of the plane of polarisation of the radio radiation from distant sources. This Faraday rotation is proportional to the strength of the magnetic field and to the electron density. Another method is to

measure the Zeeman splitting of the 21 cm radio line. These measurements have fairly consistently given a value of 10^{-10}–10^{-9} T for the strength of the interstellar magnetic field. This is about one millionth of the interplanetary field in the solar system.

16.9 Examples

Example 16.1 Estimate the dust grain size and number density in the galactic plane.

Let us compare the interstellar extinction curve in Fig. 16.4(b) with the Mie scattering curves in Fig. 16.3. We see that the leftmost parts of the curves may correspond to each other: the interval $0 < x < 5$ with $m = 1.5$ in Fig. 16.3 matches the interval $0 < 1/\lambda < 5\ \mu\text{m}^{-1}$ in Fig. 16.4(b). Remembering that $x = 2\pi a/\lambda$, this suggests a constant grain radius a, given by $2\pi a \approx 1\ \mu$m, or $a \approx 0.16\ \mu$m.

In the blue wavelength region ($\lambda = 0.44\ \mu$m), $x = 2.3$ and, according to the upper Fig. 16.3, $Q_{\text{ext}} \approx 2$. Using $A = 2$ mag for the interstellar extinction at $r = 1$ kpc, we get, substituting (16.5) into (16.7), $\overline{n} \approx 4 \times 10^{-7}\ \text{m}^{-3}$. This should give the order of magnitude of the interstellar dust density.

As a summary we could say that a considerable fraction of the interstellar extinction might be due to grains of diameter 0.3 μm and particle density of the order of $10^{-7}\ \text{m}^{-3} = 100\ \text{km}^{-3}$.

Example 16.2 Estimate the time interval between successive collisions of a hydrogen atom in interstellar gas.

Two atoms will collide if the separation between their centres becomes less than $2r$, where r is the radius of the atom. Thus, the microscopic cross section for the collision is $\sigma = \pi(2r)^2 = 4\pi r^2$. The macroscopic cross section, or the number of collisions of an H atom per unit length, is then $\Sigma = n\sigma$, where n is the number density of the H atoms. The mean free path l of an atom is the inverse of the macroscopic cross section, $l = 1/\Sigma$, and the time between two collisions is $t = l/v$, where v is the velocity of the atom.

Considering the numerical values, the Bohr radius of an H atom is $r = 5.3 \times 10^{-11}$ m. Taking $n = 1\ \text{cm}^{-3}$ we get $l = 2.8 \times 10^{13}\ \text{m} \approx 0.0009$ pc. The average velocity is not far from the root mean square velocity at $T = 125$ K, given by (5.33):

$$v = \sqrt{\frac{3kT}{m}} = 1760\ \text{m s}^{-1}.$$

These values of l and v give $t = l/v = 510$ years for the collision interval. Taking into account the velocity distribution in the gas, the mean free path appears to be shorter by a factor of $1/\sqrt{2}$, which reduces the time to about 400 years.

Example 16.3 Consider the lowest rotational transition of the CO molecule. For ^{12}CO the frequency of this line is $\nu(^{12}\text{CO}) = 115.27$ GHz, and for ^{13}CO, $\nu(^{13}\text{CO}) = 110.20$ GHz. Estimate the optical thickness of each line in a molecular cloud, where the observed brightness temperatures of the lines are $T_{\text{b}}(^{12}\text{CO}) = 40$ K and $T_{\text{b}}(^{13}\text{CO}) = 9$ K.

For the ^{12}CO line, $h\nu/k = 5.5$ K. Thus, the Rayleigh–Jeans approximation is valid if the temperature is considerably higher than 5 K. This is not always the case, but the measured value of $T_{\text{b}}(^{12}\text{CO})$ suggests that the approximation can be used.

Ignoring the background, (16.19) gives

$$T_{\text{b}} = T_{\text{exc}}\left(1 - \text{e}^{-\tau_\nu}\right).$$

The optical thickness τ_ν is proportional to the opacity or the absorption coefficient α_ν [see (4.16)], and α_ν is evidently proportional to the number of CO molecules present. Other differences between the lines are small, so we can write

$$\frac{\tau_\nu(^{12}\text{CO})}{\tau_\nu(^{13}\text{CO})} \approx \frac{n(^{12}\text{CO})}{n(^{13}\text{CO})}.$$

Adopting the terrestrial value $n(^{12}\text{CO})/n(^{13}\text{CO}) = 89$, we set

$$\tau_\nu\left(^{12}\text{CO}\right) = 89\tau_\nu\left(^{13}\text{CO}\right).$$

Assuming the excitation temperatures equal and denoting $\tau_\nu(^{12}\text{CO})$ by τ, we get

$$T_{\text{exc}}\left(1 - \text{e}^{-\tau}\right) = 40,$$

$$T_{\text{exc}}\left(1 - \text{e}^{-\tau/89}\right) = 9.$$

The solution of this pair of equations is

$$\tau_\nu\left(^{12}\mathrm{CO}\right) = 23, \qquad \tau_\nu\left(^{13}\mathrm{CO}\right) = 0.25,$$
$$T_{\mathrm{exc}} = 40\ \mathrm{K}.$$

Thus, the ^{12}CO line seems to be optically thick, and $T_{\mathrm{exc}} = T_{\mathrm{b}}(^{12}\mathrm{CO})$. If also the ^{13}CO line were optically thick, the brightness temperatures would be practically equal, and the optical thicknesses could not be determined.

16.10 Exercises

Exercise 16.1 Two open clusters, which are seen near each other in the galactic plane, have angular diameters α and 3α, and distance moduli 16.0 and 11.0, respectively. Assuming their actual diameters are equal, find their distances and the interstellar extinction coefficient a in (16.4).

Exercise 16.2 Estimate the free fall velocity on the surface of a spherical gas cloud contracting under the influence of its own gravity. Assume $n(\mathrm{H_2}) = 10^3\ \mathrm{cm}^{-3}$ and $R = 5$ pc.

Exercise 16.3 The force $\boldsymbol{F}$ exerted by a magnetic field $\boldsymbol{B}$ on a charge q moving with velocity $\boldsymbol{v}$ is $\boldsymbol{F} = q\boldsymbol{v} \times \boldsymbol{B}$. If $\boldsymbol{v}$ is perpendicular to $\boldsymbol{B}$, the path of the charge is circular. Find the radius of the path of an interstellar proton with a kinetic energy of 1 MeV. Use $B = 0.1$ nT for the galactic magnetic field.